A Novel Approach of Connected and Automated Vehicle Control and Stochastic Capacity Analysis Under On-ramp Merging Scenario

by

Tianyi Chen

A dissertation submitted in partial fulfillment of

the requirements for the degree of

Doctor of Philosophy

(Civil and Environmental Engineering)

at the

UNIVERSITY OF WISCONSIN - MADISON

2021

Date of defense examination: 12/09/2021

The dissertation is sent for review by the following members of the dissertation examination committee:

Prof. Bin Ran, Advisor, Civil and Environmental Engineering, UW-Madison

Prof. Soyoung (Sue) Ahn, Civil and Environmental Engineering, UW-Madison

Prof. David A. Noyce, Civil and Environmental Engineering, UW-Madison

Prof. Xin Wang, Industrial and System Engineering, UW-Madison

Prof. Peter J. Jin, Civil & Environmental Engineering, Rutgers University

ABSTRACT

With the substantial development of communication technology and connected and automated vehicle (CAV), vehicle merging control problem gets more in-depth research to improve traffic efficiency and safety. In this study, we proposed a systematic framework for CAV control at on-ramp merging scenario by two parts: from 1) microscopic vehicle control, to 2) macroscopic traffic capacity analysis.

For the first part, we propose a rotation-based CAV distributed cooperative control strategy for an on-ramp merging scenario. By assuming the mainline and ramp line are straight, we firstly design a virtual rotation approach that transfers the merging problem to a virtual car following (CF) problem to reduce the complexity and dimension of the cooperative CAVs merging control. Based on this concept, a multiple-predecessor virtual CF model and a unidirectional multi-leader communication topology are developed to determine the longitudinal behavior of each CAV. Specifically, we exploit a distributed feedback and feedforward longitudinal controller in preparation for actively generating gaps for merging CAVs, reducing the voids caused by merging, and ensuring safety and traffic efficiency during the process. To ensure the disturbance attenuation property of this system, practical string stability is mathematically proved for the virtual CF controllers to prohibit the traffic oscillation amplification through traffic stream. Moreover, as provision for extending the virtual CF application scenarios of any curvy ramp geometry, we utilize a curvilinear coordinate to model the two-dimensional merging control, and further design a local lateral controller based on an extended linear-quadratic regulator to regulate the position deviation and angular deviation of the lane centerlines. For the purpose of systematically evaluating the control performance of the proposed methods, numerical simulation experiments are conducted. As the results indicate, the proposed controllers can actively reduce the void and meanwhile guarantee the damping of traffic oscillations in the merging control area.

For the second part, a stochastic capacity analysis for CAV at on-ramp merging scenario has been designed to understand multiple stochastic factors' impact. By utilizing first part works, a CF capacity model and on-ramp merging capacity model based on three high-level factors including control gains, communication

capabilities, and traffic arrival pattern has been formulated. Specifically, the expected capacity and corresponding variance equations has been exploited to describe the stochastic capacity. Then, numerical simulations are conducted to illustrate the impact on different stochastic factors.

KEYWORDS

CONNECTED AUTOMATED VEHICLES

VIRTUAL CAR FOLLOWING

LONGITUDINAL CONTROL

LATERAL CONTROL

STRING STABILITY

STOCHASTIC CAPACITY ANALYSIS

MULTPLE STOCHASTIC FACTORS

ACKNOWLEDGEMENT

Throughout the writing of this dissertation, I have received a great deal of support and assistance. There are many people whom I would like to thank for their contributions, both directly and indirectly, to this thesis.

Firstly, I would like to express my deep and sincere gratitude to my research supervisor, Professor Bin Ran, whose expertise was invaluable in formulating the research questions and methodology. It was a great privilege and honor to work and study under this guidance. I am extremely grateful for what he has offered me.

I would also like to give special thanks to my dad and mom as a whole for their continuous support and understanding when undertaking my research and writing my project. Your prayer for me was what sustained me this far.

I would like to thank Dr. Yang Zhou, as my second “mentor”, for consistently encouraging me to think of what it means to be a researcher and for helping me keep perspective on where my research fits into the bigger picture. His insightful feedback pushed me to sharpen my thinking and brought my work to a higher level. I would also like to thank him for his friendship, empathy and great sense of humor.

To my lab colleagues, Dr. Shen Li, Dr. Ding Fan, Dr. Zhen Zhang, Dr. Xiaotian Li, Dr. Shuoxuan Dong, Kunsong Shi, Ran Yi, Haotian Shi, Keshu Wu, Yifan Yao, Han Cao, Xiaodan Zhang, Sicheng Fu for supporting me throughout the 5 years.

To my best friends, Yingqiao Zhou, Xiangyu Wang, Weifang Ding, Ye Zheng, Haopeng Xu, Weitao Cao, Zexia Ding, Xukanghong Sun, Zhuojun Xiao, Yong Yu for teaching me how to love.

Last but not least, I am very much thankful to my girlfriend, Huiyu Yang, for her love, understanding. Through all these darkness, she is all I see, and she is all I need. It’s because of her, I know that love can fight everything. So, MARRY ME please.

TABLE OF CONTENTS

LIST OF FIGURES

LIST OF TABLES

1. INTRODUCTION

Studies and research have determined that vehicle merging at on-ramps is one of the main critical transportation problems of traffic safety, congestion, and fuel consumption since nonsmoothed lane changing (LC) caused by different driving behaviors would trigger speed breakdowns and traffic flow oscillations. The traditional solutions to alleviate and eliminate congestions at on-ramps were related to the physical improvement of the infrastructure layout (geometric design) and active traffic management (ramp metering). With the development of advanced communication technology and paradigm shift from conventional human-driven vehicles (HDVs) to connected and automated vehicles (CAVs), the emerging technologies give researchers a great opportunity to elevate road safety and capacity to solve the merging at on-ramp problem. This chapter comes up with the general background of the study, followed by the problem statement. The objectives and the assumptions of the study are deeply discussed in the next session in order to narrow down the research goal to be more practical. The last session summarizes the outline of the paper.

1.1 Background

Traffic congestion has increased substantially over the 39 years under the records from 1982. It has become a critical road traffic problem all around the world that is affecting society, the economy, and the environment. In 2017, congestion caused people to spend 8.8 billion hours of extra travel time and to purchase an extra 3.3 billion gallons of fuel, resulting in a total cost estimated at 179 billion (KiM, 2015). Specifically, motorists lose $1.9 billion per year from lost time and wasted fuel driving on the road that is congested in Wisconsin (Mobility, 2018). In addition, traffic congestion can produce driver discomfort, distraction, and frustration, which may encourage more aggressive driving behavior and further slow the process of recovering free traffic flow. Therefore, research on the management and avoidance of this problem has been carried out since the development of freeway roads.

Vehicle merging at on-ramp is one of the major critical segments among different congestion occurrence areas including lane drops, weaving, crests, sharp bends, etc. For decades, one of the

macroscopic conventional solutions is using ramp metering to control on-ramp flows and avoid or at least delay breakdown on the mainstream. Particularly, ramp metering is the deployment of traffic signals on a ramp to restrict the on-ramp vehicles to enter the mainline for conflict reduction (Carlson et al., 2010b; Cassidy & Rudjanakanoknad, 2005; Papageorgiou et al., 1997). Although ramp metering is the direct and efficient way to control freeway networks and improve traffic conditions, it introduced a stop-and-go scenario which leads to extra energy consumption and time waste. In addition, its metering scheme whereby commuter delay is merely transferred from the freeway to its on-ramps and surface streets can be counterproductive (e.g., congestion may shift from one location to another). On the other hand, due to the uncontrollability of HDVs, this macroscopic traffic flow control method cannot eliminate the nonsmoothed LC maneuvers. Thus, the microscopic traffic control method should be considered to further improve or even solve this problem.

Substantial developments in CAV technology have been achieved during the last decade. Both connectivity and automation are integrated with CAVs, making them capable to not only drive by themselves with on-board units but also communicate with each other by vehicle-to-vehicle (V2V) communications or communicate to other facilities such as infrastructure by vehicle-to-infrastructure (V2I) communications. One of the most promising technologies using on the CAVs is cooperative adaptive cruise control (CACC) which extends adaptive cruise control with cooperative maneuvers. By sharing the vehicle information such as acceleration, speed, position, etc. through V2V communications such as Dedicated Short-Range Communications (DSRC), LTE, 5G, etc., CACC allows CAVs to obtain the following benefits: 1) driving safety is increased since actuation time is shortened; 2) roadway capacity is increased since reduction of headway between vehicles; 3) energy consumption and air pollution are reduced due to reduction of unnecessary velocity changes (Zhou et al., 2017). CACC technology has been proposed and developed over the years under different traffic networks. Specifically, this technology has been widely adopted to allow CAVs to merge with each other in a cooperative manner at an on-ramp scenario. The concept of the virtual vehicle of a CACC system in

the on-ramps cooperative merging scenario was discussed by Lu et al., (2004). The proposed approach maps a virtual vehicle onto the main road before the actual merging happens. This concept inspired some of the work in this paper which will be discussed in the following chapters.

Besides the technologies taking advantages of V2V communications, technology taking advantages of infrastructures such as infrastructure-to-vehicle (I2V) communication is another emerging approach. One of the promising automated driving systems using this technology is connected and automated vehicle highway (CAVH) (Ding et al., 2019; Ran et al., 2019). The CAVH system comprising of both CAV subsystem and connected and automated highway (CAH) subsystem. As the name implies, by installing road intelligent units (RIUs) with sensing, prediction, decision-making, and control functions on the road, the CAH subsystem has the "intelligence". Thus, the CAVH system can significantly improve transportation efficiency, traffic safety and energy consumption through the integration of CAV and CAH. Specifically, under an on-ramp scenario, CAH subsystem sends the road geometric, vehicle information, control instructions to each CAVs within the communication range. The stable RIUs on the roadside not only mitigates the computational burden of the CAVs, but also increase the stability and reliability of the entire system. These advanced technologies provide wide scenarios and platforms for various microscopic control algorithms.

1.2 Problem Statement

With the above discussion, the following issues and questions appear as part of the problem formulation:

- How to turn a complex two-dimensional vehicle merging problem to a simple one-dimensional problem?
- How to design a safe and efficient communication topology for merging maneuver?
- By actively generating gaps for merging vehicle, the cause of traffic oscillations during this process is ignored, and the method to dampen the disturbances is missing.
- The mathematical framework and methods to theoretically analyze the system stability for the merging process is missing.

- How to design a stochastic framework to estimate the CAV capacity for complex scenario?

1.3 Research Objectives

- Designs a virtual rotation approach that transfer the merging problem of straight ramp lines to a CF problem by the concept proposed by Lu et al., (2004).
- Design an upper-level controller, which uses a predetermine merge point as a reference to calculate the relative spacing for vehicle and then determines the virtual car following sequences of vehicles in a predefined merging control area.
- Design a lower-level cooperative distributed control strategy to control vehicles' trajectories with a specifically designed unidirectional multi-leader communication topology (MLT). In detail, this approach exploits a weighted multiple predecessor information based linear feedback and feedforward controller to regulate the virtual platoon spacing, and speed differences.
- Derive a mathematical proved string stability for proposed controller with sufficient conditions.
- Design a local lateral controller to extend the framework to a two-dimensional merging case. Specially, a curvilinear coordinate is utilized to describe the ramp with arbitrary shape. A local-based lateral controller is developed to control the lateral motion of CAVs, while still satisfying the concept, design, and the stability proof for the straight ramp line scenario mentioned above.
- Design a unified framework incorporating multiple factors to understand the parametric impact on stochastic capacity.

1.4 Scope and Assumption

In this study, a unified framework including CAV microscopic control and macroscopic analysis has been designed to analyze the CAV control under on-ramp merging scenario. For microscopic control, a cooperative merging control strategy is developed for CAVs at an on-ramp area which actively reduces the void and meanwhile guarantees the stability of the merging area. Specifically, given the initial position and velocity of each CAVs and the road geometric information, the following steps are conducted to fulfill control target mentioned above: 1) determine the virtual car sequencing based on

the known position and velocity of each vehicle in a centralized manner (e.g., per 1 sec); 2) design the communication topology for each vehicle according to the car sequencing order; 3) determine the acceleration portfolio for vehicles in the merging control area (e.g., 0.01 sec); 4) determine the vehicle steering angle portfolio (e.g., 0.01 sec) in the merging control area as an extension based on the step 3. The design is restricted to a pure CAV and CAH environment. And the merging geometric is consist of one lane on each road as shown in **FIG. 1-1**.

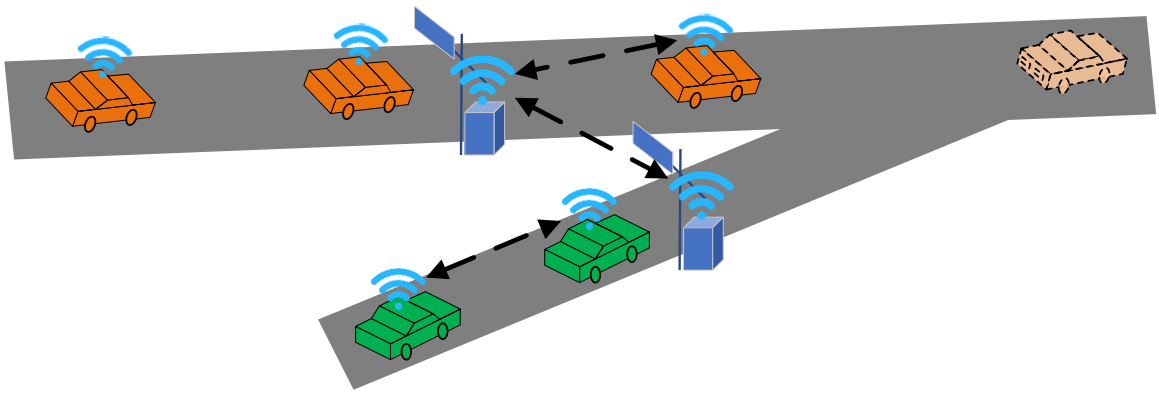

FIG. 1-1. Schematic diagram of the proposed merging at on-ramp scenario

Ahead of detailed modelling, the following assumptions have been adopted:

- The infrastructure has "intelligence" (Ding et al., 2019; Ran et al., 2019) that can sense both vehicle information and road geometrics information over a predefined merge control area.
- The CAVs are fully automated, which (SAE, 2016) means vehicle can control by themselves. Furthermore, they can communicate with each other and with infrastructure.
- Merge control area is ample enough (e.g., the control begin area is at least 250 meters away from the merging point) to apply the control strategy before vehicles merging.
- The vehicle second-order dynamics are considered for this study.
- The communication delays are negligible due to the increasing maturity of 5G communication technologies (Akpakwu et al., 2017).
- The control algorithm should obey the "First in first out" (FIFO) concept.

1.5 Dissertation Organization

The rest of this paper is organized as follows. **Chapter 2** introduces the relevant studies of CAV merging control at on-ramp scenario and macroscopic capacity analysis. **Chapter 3** utilizes a virtual rotation concept to reformulate the problem as a 'virtual' CF problem assuming the ramp is straight. Based on that, we propose a communication topology and formulate the cooperative control model on the shared virtual lane. For rigor, a string stability criterion has been mathematically proved for the 'virtual' CF problem. Then, we relax the assumption of the straightness of the ramp and develop a local lateral controller by extending the ramp scenario to a two-dimensional path coordinate. **Chapter 4** provides numerical simulation experiments to show the practicality and effectiveness of our algorithm. **Chapter 5** determined the macroscopic stochastic capacity model under both CF and on-ramp merging scenario by introducing three high-dimension factors including vehicle control gains, communication capability, and traffic arrival pattern. **Chapter 6** provides numerical analysis to show the impact of multi-scale parameters on the stochastic capacity model. Last, we give the conclusion and point out future works in **Chapter 7**.

2. LITERATURE REVIEW

2.1 On-ramp Merging Control Strategy

Vehicle merging has received broad attention during the last decades since frequent and nonsmoothed LC maneuvers significantly impact traffic safety, congestion, and fuel consumption in a merging zone and its ambient areas (Waard et al., 2009; McCartt et al., 2004; Papageorgiou et al., 2008). To mitigate the negative effect of the nonsmoothed merging, most research (Carlson et al., 2010; Sridhar et al., 2008) focuses on traffic flow control and optimization at a macroscopic level that minimizing capacity drop and improve sustainable traffic throughput.

2.1.1 Traditional Merging Strategy

One of the most conventional solutions is ramp metering which restricts the on-ramp vehicles to enter the mainline for conflict reduction and corresponded discharging rate improvement (Carlson et al., 2010b, 2010a; Cassidy & Rudjanakanoknad, 2005; Papageorgiou et al., 1997). However, due to the uncontrollability of human-driven vehicles (HDVs), the macroscopic traffic flow control methods just decrease the merging conflict by dynamically controlling the traffic flow in the merging area but cannot eliminate nonsmoothed LC maneuvers. The microscopic analysis reveals that the invasive influence of merging to the mainstream is not negligible. For example, Laval & Daganzo, (2006) claimed that LC vehicles created voids (waste spaces) in traffic streams which reduced traffic throughput from a macroscopic level. Chen & Ahn, (2018) investigated the mechanisms of how spatially distributed LCs interact with capacity-drop at a microscopic level, and the result illustrated that HDVs had the potential to create a void in merging that persists downstream due to its lower insertion speed and bounded acceleration, which led to capacity-drop. Additionally, the vehicular interaction across lanes causes disturbances. Due to the instability of HDVs car-following (CF) models, the disturbances will get amplified through vehicle string, which makes the vehicle stop and go frequently, and the phenomenon is also known as traffic oscillations significantly impacting the mainstream flow (Ahn & Cassidy, 2007; Ahn et al., 2010; Zheng et al., 2011; Li et al., 2010).

2.1.2 Upper-level Controller for CAV at On-ramp Merging

The emerging CAVs provides a great opportunity to enhance road safety and capacity to resolve the transportation problems caused by human (Rajamani et al., 2000). Specifically, CAVs brings unprecedented promises to control CAV microscopically by actively reducing the creation of voids, and further dampen traffic oscillations by cooperative adaptive cruise control (Gong & Du, 2018; M. Wang, 2018; Zhou et al., 2020; Zhou & Ahn, 2019). For the merging control, one of the very early efforts in this direction can be found in 1983, Schmidt & Posch, (1983) introduced a heuristic approach merging control algorithm for CAVs based on a two-layer controller, the upper-layer and lower-layer controllers. The upper layer determines the vehicle merging sequence, and the lower layer determines the local merging maneuvers of each vehicle. For an upper-level controller, different optimal car sequencing models have been developed. For example, Wang et al., (2007), Ntousakis et al., (2014) and Chen et al., (2020) purposed scheduling methods based on 1) distance from the merging point, 2) traveling time to the merging point, 3) the optimized future car merging sequencing with a predefined objective and constraints. Although both studies schedule the car sequence, a detailed CAV control is needed to execute the optimal sequence which rises the lower-layer controller.

2.1.3 Lower-level Controller for CAV at On-ramp Merging

The lower-level controller determines vehicle trajectories to smooth traffic and guarantee merging safety. Based on different levels of cooperation. The prevailing control algorithms can be further categorized as cooperative and non-cooperative control algorithms. The difference between these two algorithms is whether multiple-source information (predecessor vehicles) is used to control the vehicle and the degree of cooperation. For example, Kachroo & Li, (1997)and Lu et al., (2004) presented two non-cooperative single vehicle control algorithms in keeping the safe merging process and smoothing the ambient traffic flow. Specifically, Lu et al., (2004) proposed a ‘virtual platoon’ concept that projects the CAVs on both the main lane and merging lane to a virtual lane and formulate a ‘virtual platoon’ before the on-ramp merging point, which transferred the merging problem to a car-following control

issue. However, the non-cooperative control algorithm only focused on the individual vehicle optimal decisions which may induce system-level sub-optimality. The traffic disturbances analysis is ignored even though the 'virtual platoon' concept already enables the stability analysis of the traffic flow. On the other hand, due to the coordinated decision-making and multiple-source information, the cooperative control strategies have greater potentials to further improve system-level behavior and get more attention. Ran et al., (1999) and Davis, (2007) proposed a cooperative control algorithm that created gaps on the mainline large enough for vehicles with CACC function merged without speed reduction by designed CF models. Recently, several advanced control methods have been used in the designing of lower-level control, such as linear and nonlinear controllers and model predictive control (MPC). For example, Cao et al., (2015) proposed a cooperative merging path generation method using a MPC scheme to cooperate with the two vehicles on the mainline and ramp, which is closest to the merging point, to accelerate and decelerate smoothly when the merge happens. However, the influence of disturbances of the merging process on the upstream is not theoretically analyzed. Rios-Torres et al., (2015) proposed an optimal vehicle control model for multiple vehicles which targets minimizing the acceleration for safety and fuel consumption cooperatively. Further, Duret et al., (2019) developed a hierarchical control strategy for truck platooning near merging. The lower operational layer applied a MPC for multiple vehicles to actively generate gaps for vehicles to merge according to the merging sequence from the upper tactical layer and guarantee the smoothness of vehicular acceleration and deceleration. Though the local stability of the longitudinal controller has been analyzed, the stability of the entire merging section has been rarely discussed.

As cited above, most studies focus on ensuring merging safety by actively creating a gap and control the merging vehicles to reduce the void. However, they ignore the cause of traffic oscillations (e.g., caused by the cut-in maneuver and subsequently speed variation) during the process of active generation of gaps, and a corresponding method to dampen the above disturbances during this process. Especially, they lack a mathematical framework and methods to theoretically analyze the system stability for the merging process. Last but not least, the above-mentioned works treat the ramp as a

straight line, and ignore the lateral movement for vehicles, which limits the width of practical application for different merging section geometric characteristics.

2.2 Macroscopic Capacity Analysis

Similarly, as mentioned above, emerging connected and automated vehicle (CAV) technologies have been paid increasing attention in recent years since its substantial impacts on traffic safety, stability, and efficiency (Chen at el., 2017; Ghiasi et al., 2017). Compared with human-driven vehicles (HDVs), CAVs can largely improve the traffic throughput and flow stability by reducing the time headway and traffic oscillations via advanced communication technologies (e.g., vehicle-to-vehicle, vehicle-to-infrastructure) as suggested by theoretical analysis (Zhou et al., 2020; Gong & Du, 2018; Zhou et al., 2017), and numerical simulations (van Arem et al., 2006; Milanes et al., 2014). Among those merits, capacity serving as an essential indicator to describe the maximum sustainable traffic throughput, has drawn wide attention during last several years.

2.2.1 Traditional Capacity Analysis

Before we discuss the CAV capacity analysis, an understanding of conventional analysis on HDVs is indispensable. One of the earliest pioneering works can be found by Greensheilds et al., (1934), which unveiled that the capacity can be calibrated by fitting the relationship among three factors traffic speed, density, and flow, also known as the fundamental diagram (FD). Further, Highway Capacity Manual (HCM) proposed deterministic methods to estimate the capacity from speed-flow diagram under macroscopic characteristics (prevailing roadway and traffic condition). However, the constant capacity value determined from above methods are not reliable since maximum traffic flow can vary over time and space, specifically, at a traffic breakdown condition (Elefteriadou et al., 1995; Persaud et al. 1998; Lorenz & Elefteriadou 2001). Thus, in order to analyze the capacity more realistically and effectively in the congestion area, research have sought stochastic modelling from a theoretical perspective. Kuehne & Anstett (1999) and Brilon et al. (2007) both derived mathematical models of traffic flow which delivered traffic breakdown probability distribution. Their results showed high consistence with

the empirical observations. With the increasing availability of trajectory, researches have been conducted to explain the stochasticity of capacity from a microscopic driving behavior perspective (Ozguven & Ozbay, 2008., Han & Ahn, 2018). Specifically, Han and Ahn (2018) proposed a stochastic breakdown model based on driver characteristics and found that breakdown probability is sensitive to speed and minimum spacing, thus, aggressive driver could improve the traffic throughput. Apparently, above HDV capacity estimation models confine to macroscopic parameters and human driving behavior to determine the stochasticity of the road capacity, while the introduction of CAV brings new factors to the capacity stochasticity.

2.2.2 CAV Capacity Analysis

However, at current stage, there is no sufficient macroscopic empirical data to support stochastic capacity analysis on the pure CAVs, and hence we have to resort to an approach utilizing microscopic behaviors to theoretically and numerically analyze the capacity (Talebpour & Mahmassani, 2016; Milanes et al., 2014; Chen et al., 2017; Wang at el., 2016). Particularly, Chen at el., (2017) provides a capacity formulation based on platoon size and spacing characteristics, the result illustrate that the microscopic behavior of autonomous vehicles (AVs) is directly related to the macroscopic capacity. Further, Wang at el., (2016) illustrate the impact of deterministic car-following (CF) control algorithms for both AVs and CAVs on traffic flow, the results show that the CAV control model are more predictive and anticipative for traffic flow characteristic than the AV's model. Specifically, the known predecessor's microscopic driving behavior (gap and speed) increases the effective capacity. Although many literatures have derived the road capacity based on deterministic CAV CF models, the effect of stochasticity of microscopic factors on capacity has rarely been addressed.

Similar to HDVs, CAVs CF controllers also exhibit stochastic characteristics. The difference between those two CF behaviors is that the stochasticity of HDV car following is mainly introduced by human control, perception, reaction differences, which can be concluded as human behavior differences, while the stochasticity of CAVs CF control come from communication, and parametric stochasticity for CAV

controllers. Current CAV CF controllers mainly stick to constant time gap policies and based on that, linear controllers (Morbidi et al., 2013; Zhou & Ahn, 2019), model predictive controllers (Wang et al., 2013; Gong et al., 2016; Zhou et al., 2017a), and deep reinforcement learning controllers (Shi et al., 2021) are developed. Among those control algorithms, linear controllers are widely adopted due to their analytical forms and string stability guarantee, which is an important property to attenuate the disturbances through vehicle string. For linear controllers, Zhou and Ahn (2019) has proposed a robust CF control and derived sufficient conditions for both local and string stability by introducing the uncertainty of the vehicle dynamics and communication delays. Meanwhile, Wang et al., (2020) investigate the influence of information flow topology and different vehicle dynamic control parameters on cooperative adopted cruise control. Although these literatures have studied the parametric stochasticity of their controllers, they have not further explored corresponding impact on road capacity. All the parameters such as communication capabilities, and control boundaries contribute to CAV CF behavioral stochasticity and further render the stochasticity of CAV capacity.

Moreover, with the maturity of one-dimensional CF research, more literatures extend their studies to two-dimensional CAV control under complex scenarios such as intersection, merging, and diverging (Cao et al., 2015; Duret et al., 2019; Chen et al., 2021). Specifically, Chen et al., (2021) proposed a rotation-based CAV distributed cooperative control strategy for an on-ramp merging scenario. A communication topology design and virtual CF model has been designed based on a virtual rotation concept. The proposed virtual CF model exploit a distributed feedback and feedforward controller to reduce the voids caused by merging, ensure safety and disturbance attenuation. Based on the pure CAV environment and the proposed analytical linear controller, the capacity analysis of a highway on-ramp section depends entirely on the corresponding communication capabilities, vehicle control boundaries, safety parameters, and traffic arrival patterns. Thus, the concept and method inspire the work we have done in this paper.

To the authors best knowledge there is no previous research addressing the stochastic capacity analysis for the pure automated driving environment on complex scenarios. Some CF studies above only

consider the impact of the deterministic vehicle control algorithm on the road capacity (Chen et al., 2017; Wang et al., 2021). While some studies consider the stochasticity of the microscopic control parameters but ignore the impact on the macroscopic capacity. Thus, no literatures have systematically studied the capacity impact from the stochasticity of the vehicle control parameters and proposed any corresponding stochastic capacity model. Not to mention that the relevant research on complex scenarios is completely missing. Thus, under the trends to connected and automated driving, it is necessary to estimate and analyze the capacity of pure CAV environment on a highway on-ramp scenario.

3. CAV CONTROL STRATEGY UNDER ON-RAMP MERGING

Motivated by the above research gaps, in this chapter, we firstly design a virtual rotation approach that transfers the merging problem of straight ramp lines to a CF problem by the concept proposed by Lu et al., (2004). This concept has been extended in Xu et al., (2018) at an unsignalized intersection which further inspired us to systematically design the virtual rotation approach. Thus, the rotation process, which serves as an upper-level controller, uses a predetermine merge point as a reference to calculate the relative spacing for vehicle and then determines the virtual car following sequences of vehicles in a predefined merging control area. A lower-level cooperative distributed control strategy is proposed to control vehicles' trajectories with a specifically designed unidirectional multi-leader communication topology (MLT). In detail, this approach exploits a weighted multiple predecessor information-based linear feedback and feedforward controller to regulate the virtual platoon spacing and speed differences. The string stability for the proposed controller is further mathematically proven. To generalize the application scenario, this study extends the framework to a two-dimensional case by considering CAVs lateral movement. Specifically, a curvilinear coordinate is utilized to describe the ramp with arbitrary shape. A local-based lateral controller is developed to control the lateral motion of CAVs, while still satisfying the concept, design, and the stability proof for the straight ramp line scenario mentioned above.

3.1 Control System Modelling

The first session describes the design and formulation of the proposed cooperative merging control strategy for a simple scenario where the mainline and ramp line are straight. A virtual rotation strategy has been introduced to reduce modeling complexity. Specifically, this study rotates CAVs on mainline (Y_1-axis) and CAVs on on-ramp (Y_2-axis) to a shared straight axis Z, as it shown in **FIG. 3-1**. A virtual CF sequence is obtained by the rotation strategy and FIFO scheme. To leverage the V2V communication among multi-vehicles, a unidirectional multi-leader communication topology is proposed in this research. According to the rules of sequence and topology, a multi-predecessor linear

feedback and feedforward controller has been exploited to alleviate the disturbances on the gap generation and merging procedure.

3.1.1 Virtual Rotation and Virtual Car Following Sequencing

To distinguish the CAVs, we define two groups of sets for CAVs on mainline (i.e., $I_M = \{1_M, 2_M, \ldots m_M\}$) and on-ramp (i.e., $I_R = \{1_R, 2_R, \ldots r_R\}$), respectively. Each group of sets contains a vehicle sequence set, a vehicle position set and a vehicle velocity set, which denoted as $X_M = \{x_1, x_2, \ldots, x_m\}, X_M \in \mathbb{R}^m$, $V_M = \{v_1, v_2, \ldots, v_m\}, V_M \in \mathbb{R}^m$, $X_R = \{x_1, x_2, \ldots, x_r\}, X_R \in \mathbb{R}^r$, $V_R = \{v_1, v_2, \ldots, v_r\}, V_R \in \mathbb{R}^r$.

Based on the vehicles' state information, we define the concept of 'virtual rotation' as the process determining the car-following sequence of merging, which is equivalent to finding the optimal car following sequence for vehicles in a virtual axle based on a predefined law. The importance of the maneuver lies in reducing modelling complexity and convert the merging problem to a car following problem, which makes the string stability analysis available. One of the simplest strategies is sorting the car following sequence based on the relative distance to the merging point. Specifically, we rotate the on-ramp y_2-axis to the mainline y_1-axis and construct a virtual Z-axis, while maintaining the physical distance to the merge point as illustrated by **FIG 3-1**. Based on that, we can have a union of vehicles index, relative position, and speed set on the virtual axis Z, as below:

$$X_Z = X_M \cup X_R, \tag{1a}$$

$$V_Z = V_M \cup V_R, \tag{1b}$$

$$I_Z = I_M \cup I_R. \tag{1c}$$

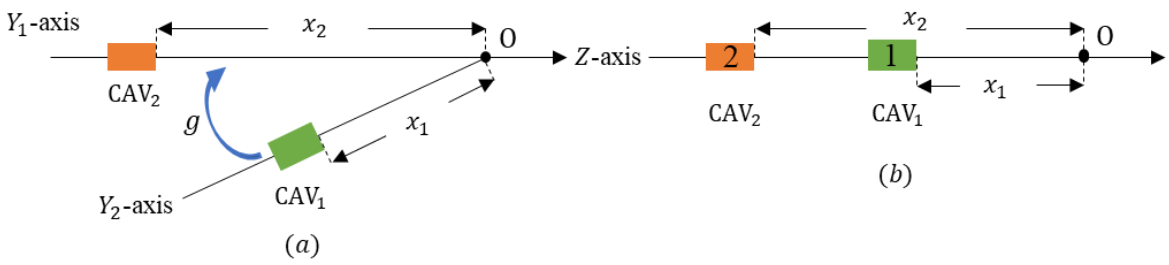

FIG. 3-1. An example of the proposed virtual rotation approach in (a) Y_1-axis, Y_2-axis, (b) virtual Z-axis

Correspondingly, based on the CAVs' index and positions on the Z-axis, we can easily get the virtual car-following sequences on Z-axis by a function g which sorts X_Z in a monotonically descending order:

$$(\tilde{X}_Z, \tilde{V}_Z, \tilde{I}_Z, \tilde{F}_Z) = g(X_Z, V_Z, I_Z), \tag{2}$$

where $\tilde{X}_Z, \tilde{V}_Z, \tilde{I}_Z, \tilde{F}_Z$ represent the relative position set, speed set, car following sequence set, the ramp/mainline indicator set on Z-axis after sorting. $\tilde{I}_Z$ is organized in an ascending order $\tilde{I}_Z = \{1,2,\dots,N_{total}\}$, $N_{total} = M + R$, $\tilde{F}_Z = \{f_{Z,1}, \dots f_{Z,N_{total}}\}$. Specifically, for $i \in \tilde{I}_Z$, we let $f_{Z,i} = 1$, if the i^{th} vehicle on the virtual axis Z is actually on the mainline, and $f_{Z,i} = 0$ vice versa. Though this virtual rotation maneuver may result in violation of safety in the virtual axle, the vehicles which have safety violation are actually at different lanes. Further, since the rotation process sequences all vehicles in the merging area, the vehicles on the mainline and ramp line will only have equal or large desired spacing. Note that, g can be any function satisfying FIFO, such as Chen et al., (2020) can be applied to our framework. Since this section is not the main focus of this study, we just utilized a very simple strategy as Eq. (2).

3.1.2 Communication Topology Design

According to above virtual car-following sequence, we specifically design a unidirectional multi-leader communication topology (MLT) to leverage the V2V communication among multi-vehicles and prevent the collisions between adjacent cars on both mainline and ramp entrances. The communication topology will further facilitate the strict string stability for the vehicles on the mainline and ramp respectively, later given in following session.

The MLT on the virtual Z-axis is modeled with a directed graph $\mathcal{G}(\tilde{I}_Z, \mathcal{E}, \mathcal{A})$, where $\tilde{I}_Z$ represents the vertices of the graph, whose number of vertices is N_{total}. $\mathcal{E} \subseteq \tilde{I}_Z \times \tilde{I}_Z$ is the set of edges representing the car following connections between each pair of following vehicles. The adjacency matrix $\mathcal{A} =$

$[a_{i,j}], \forall i,j \in \tilde{I}_Z$, represents the communication connections. We specifically let a complementary communication set as $\mathcal{E}_c$ connecting vertices $\forall i,j \in \tilde{I}_Z$, and $i < j$, defined as: $\mathcal{E}_c = \cup\{edge\ (i,j)\}$ if $f_{Z,i} = f_{z,j}$ & ∃ i < k < j, $f_{z,k} = f_{z,i}$ or $f_{Z,i} \neq f_{z,j}$ & ∃ i < k < j, $f_{z,k} = f_{z,j}$. The edge set $\mathcal{E}$ is defined as:

$$\mathcal{E} = \{\tilde{I}_Z \times \tilde{I}_Z\} \backslash \mathcal{E}_c \tag{3}$$

And the $\mathcal{A}$ can be defined as:

$$\begin{cases} 1, if\{\mathcal{E}_{i,j} \in \mathcal{E}\}, \\ 0, otherwise, \end{cases} i,j \in N_{total}, \tag{4}$$

where $\mathcal{E}_{i,j} \in \mathcal{E}$ Similarly, means that vehicle j can receive the information of vehicle i.

To clearly understand the definition of Eq. (3), we summarize it as the thumb of rules below: 1) for vehicle i and predecessor j with the same ramp/mainline indicator if there is a vehicle k between i and j that has the same indicator as vehicle i, no communication is allowed between i and j; 2) for vehicle i and predecessor j with the different indicator, if there is a vehicle k between i and j that has the same indicator as predecessor j, no communication is allowed between i and j. Other than the two above scenarios, CAVs are all unidirectional interconnected. An intuitive example has been provided in **FIG. 3-2** to illustrate how CAVs communicate in both virtual and real-world scenes. This example contains 5 CAVs, 3 on the mainline, 2 on the on-ramp, and the virtual car-following sequence has been determined as $\tilde{F}_Z = \{1,0,0,1,0\}$. Based on the MLT rules, the fifth vehicle (the last mainline vehicle passing the merging point) can only communicate with its two predecessors. No communication is allowed with the second and first CAV since the third CAV already has the same mainline indicator as the fifth one. Similarly, the fourth CAV can receive information from its three predecessors until the first vehicle since the first vehicle has the same on-ramp indicator.

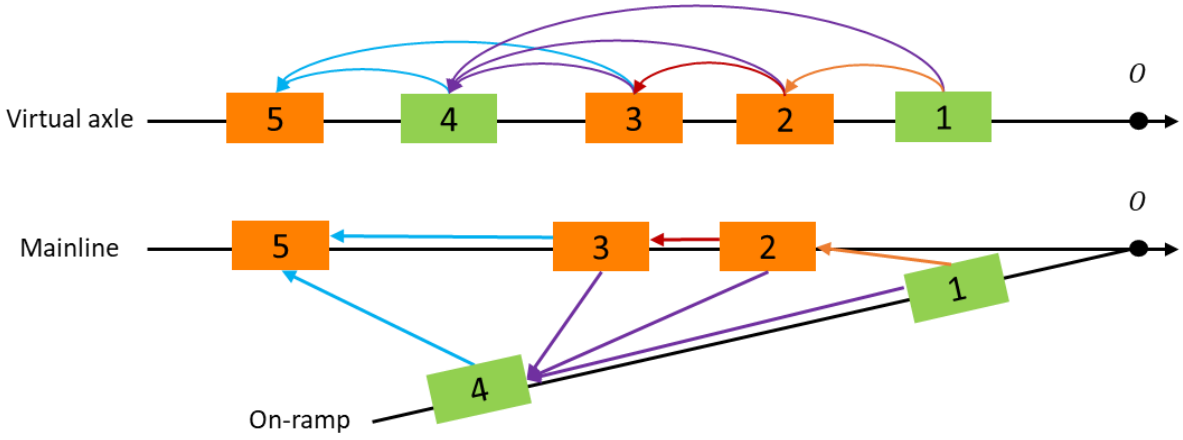

FIG. 3-2. An example of MLT in both virtual and real-world scene

3.1.3 Longitudinal Control Structure

The merging problem can be converted to a virtual CF control problem by virtual rotation and virtual car following sequencing. Specifically, the control objective is to coordinate CAVs on-ramp and mainline to actively generate the gap for vehicles to merge, reduce the voids, and meanwhile reduce traffic oscillations during the whole process. Based on the rotation scheme developed above, we design a linear feedback and feedforward controller on the basis of Wang et al., (2020) for vehicles within each subset.

The schematic of the feedback and feedforward controller for vehicle i is illustrated in **FIG. 3-3**. U_i represents the control command, which consists of two feedback control components $U_{b,i}$: 1) the spacing error E_i , 2) the velocity difference ΔV_i, and one feedforward control term $U_{f,i-k}$ from the acceleration rates $\ddot{x}_{i-k}$ of every predecessors from vehicle $i-1$ to $i-k$. G_i and M_i are the ideal longitudinal vehicle dynamics, X_i and V_i represents the position and velocity output of vehicle i, H_i denotes the constant time gap (CTG) spacing policy, and $\omega_{e,i}$ and $\omega_{v,i}$ are the equilibrium spacing coefficient and equilibrium velocity coefficient, $\alpha_{f,k}$ and $\alpha_{b,k}$ are the weighting coefficients for acceleration feedback and feedforward information, $\gamma_{b,k}$ is the weighting coefficient for velocity feedback information. These three coefficients represent the relative importance of the information from k predecessors to vehicle i and are different from each case which are discussed in the following

sessions.

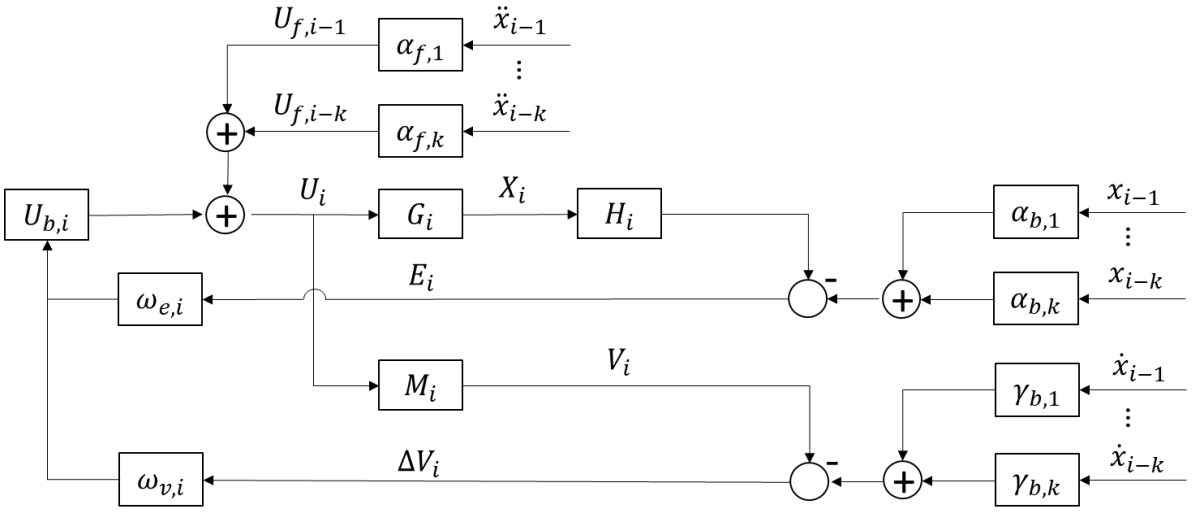

FIG. 3-3. Schematic of the feedback and feedforward controller

Since this study considers an idealized longitudinal vehicle dynamics model that ignoring air drag and actuator delay, for the lower-level controller, we assume it can address vehicle internal dynamics so that vehicle can respond to acceleration and velocity commands without any delays, which is widely used in the literatures, e.g., (Wang et al., 2020; Zhou et al., 2017). The linearized state-space representation of the idealized longitudinal vehicle dynamics can be represented as:

$$\begin{cases} \dot{x}_i(t) = v_i(t), \\ \dot{v}_i(t) = u_i(t), \end{cases} \tag{5}$$

where $x_i(t)$, $v_i(t)$ and $u_i(t)$ are the absolute position, velocity and acceleration of vehicle i at time t. To analyze stability performance, the modeling and analysis are performed in the Laplace domain. The idealized longitudinal vehicle dynamics model in Laplace domain can be described by using transfer functions as:

$$G_i(s) = X_i(s)U_i(s)^{-1} = s^{-2}, \tag{6a}$$

$$M_i(s) = V_i(s)U_i(s)^{-1} = s^{-2}, \tag{6b}$$

where the input $U_i(s)$ denotes the acceleration of vehicle i and the output $X_i(s)$ and $V_i(s)$ denotes the absolute position and velocity of vehicle i in the Laplace domain.

To achieve more efficient damping oscillations, we obtain the desired relative distance between vehicle i and its N_i predecessors, whose communications are active, using the CTG policy as follows:

$$d_{i,k}(t) = N_i[L + \tau \dot{x}_i(t)] \tag{7}$$

where $d_{i,k}(t)$ is the desired relative distance between vehicle i and vehicle k, and τ is the desired time gap for vehicle i. L is the constant standstill distance (including vehicle length) between the two adjacent vehicles, $\dot{x}_i(t)$ is the velocity of vehicle i.

The convex combination of spacing errors as follows:

$$e_i(t) = \sum_{k=1}^{N_i} \alpha_{b,k}\{[(x_{i-k}(t) - x_i(t)] - d_{i,k}(t)\}, \tag{8}$$

$s.t.$

$$\sum_{k=1}^{N} \alpha_{b,k} = 1, \tag{9}$$

where $\alpha_{b,k}$ is the weighting coefficients for position feedback information.

Substituting Eq. (7) into Eq. (8), the weighted spacing error is

$$e_i(t) = \sum_{k=1}^{N_i} \alpha_{b,k}\{[(x_{i-k}(t) - x_i(t)] - k[L + \tau \dot{x}_i(t)]\}. \tag{10}$$

Taking the Laplace transformation of Eq. (10), the spacing error can be expressed equivalently as:

$$E_i(s) = \sum_{k=1}^{N_i} \alpha_{b,k}\{[(X_{i-k}(s) - X_i(s)] - k\tau s X_i(s)\} \tag{11}$$

$$= \sum_{k=1}^{N_i} \alpha_{b,k} X_{i-k}(s) - X_i(s)\left(1 + \sum_{k=1}^{N_i} \alpha_{b,k} k\tau s\right)$$

$$= \sum_{k=1}^{N_i} \alpha_{b,k} X_{i-k}(s) - H_i(s) X_i(s),$$

where $H_i(s)$ is the CTG spacing policy in frequency domain, given by:

$$H_i(s) = 1 + \sum_{k=1}^{N_i} \alpha_{b,k} * k * \tau * s. \tag{12}$$

The equilibrium velocity of vehicle i with its N_i predecessors can be represented as:

$$v_{i,e}(t) = \sum\nolimits_{k=1}^{N_i} \gamma_{b,k} v_{i-k}(t), \tag{13}$$

$s.t.$

$$\sum\nolimits_{k=1}^{N_i} \gamma_{b,k} = 1, \tag{14}$$

where $\gamma_{b,k}$ is the weighting coefficient for velocity feedback information. Then, the deviation from equilibrium velocity of vehicle i can be expressed as:

$$\Delta v_{i,e}(t) = v_i(t) - v_{i,e}(t). \tag{15}$$

Taking the Laplace transformation of Eqs. (13) and (15), we have:

$$V_{i,e}(s) = \sum\nolimits_{k=1}^{N_i} \gamma_{b,k} V_{i-k}(s). \tag{16}$$

$$\Delta V_{i,e}(s) = V_i(s) - \sum_{k=1}^{N_i} \gamma_{b,k} V_{i-k}(s). \tag{17}$$

The control command consists of a feedback term (spacing error feedback and velocity feedback) and a set of feedforward terms, which shown as follow:

$$U_i(s) = U_{b,i}(S) + \sum_{k=1}^{N_i} U_{f,i-k}(S), \tag{18}$$

where the feedback term $U_{b,i}(S)$ uses spacing error and velocity to stabilize the closed-loop system while the feedforward term $U_{f,i-k}(S)$ uses acceleration rates from the N_i predecessors to minimize the spacing error.

The feedback term $U_{b,i}(S)$ and the corresponding feedback controller are defined as:

$$U_{b,i}(S) = \omega_{e,i} E_i(s) + \omega_{v,i} \Delta V_{i,e}(s), \tag{19}$$

where $E_i(s)$ is the spacing error in the Laplace domain in Eq. (11). $\omega_{e,i}$ and $\omega_{v,i}$ are the feedback gains for deviation from equilibrium spacing and equilibrium speed respectively, where larger feedback gains will make vehicle react more intensively.

The feedforward terms $U_{f,i-k}(S)$ indicate that the acceleration rates of vehicle $i-k$ are defined as:

$$U_{f,i-k}(S) = \alpha_{f,k}\, s^2 X_{i-k}(s). \tag{20}$$

The overall control command is obtained by summing up Eqs. (18), (19) and (20). Through inverse Laplace transformation, the expression for the control command is:

$$U_i(t) = \omega_{e,i} e_i(t) + \omega_{v,i} \Delta v_{i,e}(t) + \sum_{k=1}^{N_i} \alpha_{f,k}\, \ddot{x}_{i-k}(t). \tag{21}$$

3.2 String Stability Criterion

In this session, we analyze the string stability for longitudinal controller under the MLT mentioned in **Chapter 3.1.2**. Specifically, we mathematically define the property of string stability and derive sufficient conditions by analysis method. Since the velocity of the vehicle i is affected by its multiple predecessors, we consider the following definition of strictly L_2 norm string stability based on (Darbha et al., 2017):

Definition 1. A CAV platoon is (practically) L_2 norm string stable if and only if:

$$\|v_i(t)\|_2^2 \leq \frac{1}{N_i}\sum_{k=1}^{N_i}\|v_{i-k}(t)\|_2^2\,, \tag{22}$$

where $v_i(t)$ is the absolute velocity of vehicle i on virtual Z-axis. $\|v_i(t)\|_2^2 = \int_{-\infty}^{+\infty}|v_i(t)|^2\,dt$ is the square of the L_2 norm of v_i. According to Eq. (22), it requires that the square of the L_2 absolute velocity of vehicle i is attenuated in the sense that it is less than the average of the squares of its predecessors' L_2 absolute velocities. Note that, in the following study, we treat the square of the L_2 absolute velocity as energy for easy understanding.

To analyze the frequency domain behavior of our system, we conduct the Fourier transformation on the system by Eqs. (11) and (21). The result is shown in Eq. (23).

$$\begin{aligned} s^2X_i(s) = \omega_{e,i}\left[\sum_{k=1}^{N_i}\alpha_{b,k}X_{i-k}(s) - H_i(s)X_i(s)\right] + \omega_{v,i}s\left[X_i(s) - \sum_{k=1}^{N_i}\gamma_{b,k}X_{i-k}(s)\right] \\ + s^2\sum_{k=1}^{N_i}\alpha_{f,k}\,X_{i-k}(s). \end{aligned} \tag{23}$$

To simplify the further analysis, we define $Q_k(s) = \frac{P_k(s)}{J_k(s)}$, where $J_k(s) = s^2 + \omega_{e,i}H_i(s) - s\omega_{v,i}$, and $P_k(s) = \omega_{e,i}\alpha_{b,k} - s\omega_{v,i}\gamma_{b,k} + s^2\alpha_{f,k}$. Then, Eq. (23) can be represented as:

$$X_i(s) = \sum_{k=1}^{N_i} Q_k(s)\, X_{i-k}(s). \tag{24}$$

By dividing s on both hand sides of Eq. (24), we can have:

$$V_i(s) = \sum_{k=1}^{N_i} Q_k(s)\, V_{i-k}(s). \tag{25}$$

Based on Definition 1, and Eq. (25), the Proposition 1 can be got as below:

Proposition 1. If $\|Q_k(j\omega)\|_\infty \leq \frac{1}{N_i}$, the CAV platoon is string stable on the virtual Z-axis.

Proof. According to the Parseval's theorem (Steele, 2004), the energy in time and frequency domain are equal, and then we have:

$$\begin{aligned} \|v_i(t)\|_2^2 &= \int_{-\infty}^{+\infty} |v_i(t)|^2\, dt = \int_{-\infty}^{+\infty} |V_i(j\omega)|^2\, d\omega \\ &= \int_{-\infty}^{+\infty} \left| \sum_{k=1}^{N_i} (Q_k(j\omega) V_{i-k}(j\omega)) \right|^2 d\omega. \end{aligned} \tag{26}$$

According to the Cauchy-Schwarz inequality (Steele, 2004), we can get,

$$\begin{aligned} \|v_i(t)\|_2^2 &\leq \int_{-\infty}^{+\infty} \left(N_i \sum_{k=1}^{N_i} (V_{i-k}^T(j\omega) Q_k^T(j\omega) Q_k(j\omega) V_{i-k}(j\omega)) \right) d\omega \\ &\leq N_i \sum_{k=1}^{N_i} \left((sup_\omega |Q_k(j\omega)|)^2 \cdot \int_{-\infty}^{+\infty} V_{i-k}^T(j\omega) V_{i-k}(j\omega) d\omega \right) \\ &= N_i \sum_{k=1}^{N_i} (\|Q_k(j\omega)\|_\infty^2 \cdot \|v_{i-k}(t)\|_2^2). \end{aligned} \tag{27}$$

To satisfy Definition 1, by substituting Eq. (27) into (22), we can have:

$$\|Q_k(j\omega)\|_\infty \leq \frac{1}{N_i}, \forall\, 1 \leq k \leq N_i. \tag{28}$$

Next, we bring the Eq. (28) proposed by proposition 1 into the two cases we defined below:

1. *The Equally Weighted Case:*

We firstly begin with Case 1 where weighted coefficients are equal to $\frac{1}{N_i}$ similar to (Bian et al., (2019), which shows below in Eq. (29). The exact identical coefficients are for dimensionality reduction which neat the parameters and control algorithm. And the assignment of equally weight is to demonstrate that we treat every coefficient under each k is equally important.

$$\alpha_{b,k} = \alpha_{f,k} = \gamma_{b,k} = \frac{1}{N_i}. \tag{29}$$

Proposition 2. The CAV platoon is string stable on the virtual Z-axis, if the following inequality equation are satisfied:

$$\left(\omega_{e,i}\tau\frac{(1+N_i)}{4}\right) - \omega_{v,i} \geq 0. \tag{30}$$

Proof. By substituting Eq. (29) into Eq. (28), we can get:

$$\|Q_k(j\omega)\|_\infty = \left\|\frac{P_k(j\omega)}{J_k(j\omega)}\right\|_\infty = \left\|\frac{\omega_{e,i}\alpha_{b,k} - j\omega\omega_{v,i}\gamma_{b,k} - \omega^2\alpha_{f,k}}{-\omega^2 + \omega_{e,i}(1 + \sum_{k=1}^{N_i}\alpha_{b,k} * k\tau j\omega) - j\omega\omega_{v,i}}\right\|_\infty \tag{31}$$

$$= \left\|\frac{\frac{1}{N_i}\omega_{e,i} - \frac{1}{N_i}\omega^2 - \frac{1}{N_i}\omega_{v,i}j\omega}{-\omega^2 + \omega_{e,i} + \left(\left(\omega_{e,i}\tau\frac{(1+N_i)}{2}\right)\omega - \omega\omega_{v,i}\right)j}\right\|_\infty \leq \frac{1}{N_i}.$$

By multiply N_i on both hand sides of Eq. (31) and simplified to $\left\|\frac{A+Bj}{C+Dj}\right\|_\infty \leq 1$, we have:

$$A = \omega_{e,i} - \omega^2, \tag{32a}$$

$$\mathrm{B} = -\omega\omega_{v,i}, \tag{32b}$$

$$\mathrm{C} = -\omega^2 + \omega_{e,i}, \tag{32c}$$

$$D = \left(\omega_{e,i}\tau\frac{(1+N_i)}{2}\right)\omega - \omega\omega_{v,i}. \tag{32d}$$

Then, the Eqs. (32a)–(32d) can be simplified as $\mathrm{A}^2 + \mathrm{B}^2 \leq \mathrm{C}^2 + \mathrm{D}^2$, which is shown below:

$$\begin{aligned} &{\omega_{e,i}}^2 + \omega^4 - 2\omega^2\omega_{e,i} + \omega^2{\omega_{v,i}}^2 \\ &\qquad \leq \left({\omega_{e,i}}^2\tau^2\frac{(1+N_i)^2}{4}\right)\omega^2 + \omega^2{\omega_{v,i}}^2 - \left(\omega_{e,i}\tau(1+N_i)\right)\omega^2\omega_{v,i} \\ &\qquad + \omega^4 + {\omega_{e,i}}^2 - 2\omega^2\omega_{e,i} \Longrightarrow \left(\omega_{e,i}\tau\frac{(1+N_i)}{4}\right) - \omega_{v,i} \geq 0. \end{aligned} \tag{33}$$

In special case scenario, when $N_i = 1$, Eq. (33) can be expressed as:

$$\frac{\omega_{e,i}\tau}{2} - \omega_{v,i} \geq 0. \tag{34}$$

2. The Non-equally Weighted Case:

We extended the case 1 to a more general and realistic case where the weighted coefficients are assigned by a function of k and N_i which shows below in Eq. (35). The assignment function is to show that the closer to CAV_i, the greater the weighted coefficient of the CAV and the greater the impact on CAV_i.

$$\alpha_{b,k} = \alpha_{f,k} = \gamma_{b,k} = \begin{cases} \dfrac{1}{2^k}, & 1 \leq k \leq N_i - 1 \\ \dfrac{1}{2^{N_i-1}}, & k = N_i \end{cases}. \tag{35}$$

Theorem 1 (Darbha et al., 2019) The string stability for the system with the form as Eq. (25) is string stable if the following inequality is satisfied:

$$\sum_{k=1}^{N_i} \|Q_k(j\omega)\|_\infty \leq 1. \tag{36}$$

Proposition 3. The CAV platoon is string stable on the virtual Z-axis, if the following inequality equation are satisfied:

$$\omega_{e,i}\tau\theta - 2\omega_{v,i} \geq 0. \tag{37}$$

Proof. By substituting Eq. (35) into (36), we can have:

$$\sum_{k=1}^{N_i} \|Q_k(j\omega)\|_\infty = \left\| \frac{\omega_{e,i}\alpha_{b,k} - j\omega\omega_{v,i}\gamma_{b,k} - \omega^2\alpha_{f,k}}{-\omega^2 + \omega_{e,i}\left(1 + \sum_{k=1}^{N_i} \alpha_{b,k} * k\tau j\omega\right) - j\omega\omega_{v,i}} \right\|_\infty \leq \sum_{k=1}^{N} \alpha_{b,k}. \tag{38}$$

By dividing $\sum_{k=1}^{N_i} \alpha_{b,k}$ on both hand side of Eq. (38) and simplified to $\left\|\frac{A+Bj}{C+Dj}\right\|_\infty \leq 1$, we have:

$$A = \omega_{e,i} - \omega^2, \tag{39a}$$

$$\mathrm{B} = -\omega\omega_{v,i}, \tag{39b}$$

$$\mathrm{C} = -\omega^2 + \omega_{e,i}, \tag{39c}$$

$$D = \left(\omega_{e,i}\tau\theta\right)\omega - \omega\omega_{v,i}, \tag{39d}$$

$$\theta = \sum_{k=1}^{N_i} \alpha_{b,k} * k. \tag{39f}$$

Then, the Eqs. (39a)–(39f) can be simplified as $\mathrm{A}^2 + \mathrm{B}^2 \leq \mathrm{C}^2 + \mathrm{D}^2$, which is shown below:

$$\begin{aligned} &{\omega_{e,i}}^2 + \omega^4 - 2\omega^2\omega_{e,i} + \omega^2{\omega_{v,i}}^2 \\ &\qquad \leq \left({\omega_{e,i}}^2\tau^2\theta^2\right)\omega^2 + \omega^2{\omega_{v,i}}^2 - 2\omega^2\omega_{e,i}\omega_{v,i}\tau\theta + \omega^4 + {\omega_{e,i}}^2 \\ &\qquad - 2\omega^2\omega_{e,i} \Longrightarrow \omega_{e,i}\tau\theta - 2\omega_{v,i} \geq 0. \end{aligned} \tag{40}$$

Remark 1. According to Wang et al., (2020), with the worst-case scenario where the $\frac{V_{i-k}(s)}{V_{i-N}(s)}, \forall\, 1 \leq$

$k < N$ is equal to one (which means the traffic oscillation is neither amplified nor dampened), the transfer function in Eq. (25) becomes:

$$V_i(s) = V_{i-N}(s) \sum_{k=1}^{N_i} Q_k(s). \tag{41}$$

By Cauchy-Schwarz inequality, we have:

$$\|V_i(s)\|_2 \leq \left\| \sum_{k=1}^{N_i} Q_k(s) \right\|_\infty \|V_{i-N}(s)\|_2. \tag{42}$$

In order to satisfy the head-to-tail string stability (Wang, 2018), $\frac{\|V_i(s)\|_2}{\|V_{i-N}(s)\|_2} \leq 1$, which gives the sufficient condition as $\left\|\sum_{k=1}^{N_i} Q_k(s)\right\|_\infty \leq 1$ based on Eq. (42). Further, since

$$\sum_{k=1}^{N_i} \|Q_k(j\omega)\|_\infty \leq \left\| \sum_{k=1}^{N_i} Q_k(s) \right\|_\infty \leq 1, \tag{43}$$

we can find that practical string stability conditions given by Eq. (28) and Eq. (36) is more stringent, and hence the head-to-tail string stability can be naturally satisfied. By the communication topology in **Chapter 3.1.2** we can further conclude that the CAV platoon on both mainline and on-ramp is strictly string stable.

3.3 Two-Dimension Coordinate Extension

To increase the application on all road geometries, we extend the ideal merging scenario whose ramp is a straight line to a general scenario, a two-dimensional case. A local lateral controller is designed to regulate the vehicles' deviation from the lane centerline based on the proposed longitudinal control. We firstly describe the vehicle state in a curvilinear coordinates model and illustrate the vehicle lateral dynamics. The local linear feedback and feedforward controller are designed based on an

extended linear quadratic regulator (ELQR). Note that to make the system more realistic, both holonomic and nonholonomic vehicle lateral movement system has been considered in this study.

3.3.1 Curvilinear Coordinates Model

In this paper, we use a curvilinear coordinates model rather than a Cartesian coordinate model to model the vehicle kinematics of the lateral movements. Certainly, the Cartesian coordinate model can easily express the distance between the cars and the merging point. However, to express the vehicle trajectory (including steering angle, position, and distance) more accurately and conveniently to the centerline of the curved on-ramp, the curvilinear coordinate model is introduced. Since both coordinate models can be invertible transformed by each other, the curvilinear coordinates model given by **FIG. 5-1**., can be represented as $[p_x, p_y, \theta]^S \in R^3$: where its position is $[p_x, p_y]$, and θ is the orientation in the global frame. Then, the vehicle state $M(t)$ can be represented in a curvilinear coordinate $[x_i(t), r_i(t), \Delta\theta_i(t)]^T$, where the vehicle state contains the path length (curvilinear abscissa) at the closest point, $x_i(t)$, lateral deviation $r_i(t)$, the angular deviation $\Delta\theta_i(t)$ which can be expressed as:

$$M_i(t) = \begin{bmatrix} x_i(t) \\ r_i(t) \\ \Delta\theta_i(t) \end{bmatrix}, \tag{44}$$

where $r_i(t)$ is the orthogonal distance from the center of the CAV to the closest point on the on-ramp y_2-axis, and $\Delta\theta_i(t) = \theta_i(t) - \theta_{des(i)}(t), \theta_i(t)$ is the angle between the CAV heading direction and the x-axis, $\theta_{des(i)}(t)$ is the angle between the tangent of the road centerline and the x-axis in the global frame. An example of Two CAVs under our scenario in Path coordinate system is shown in **FIG.** Error! R eference source not found.**-1**.

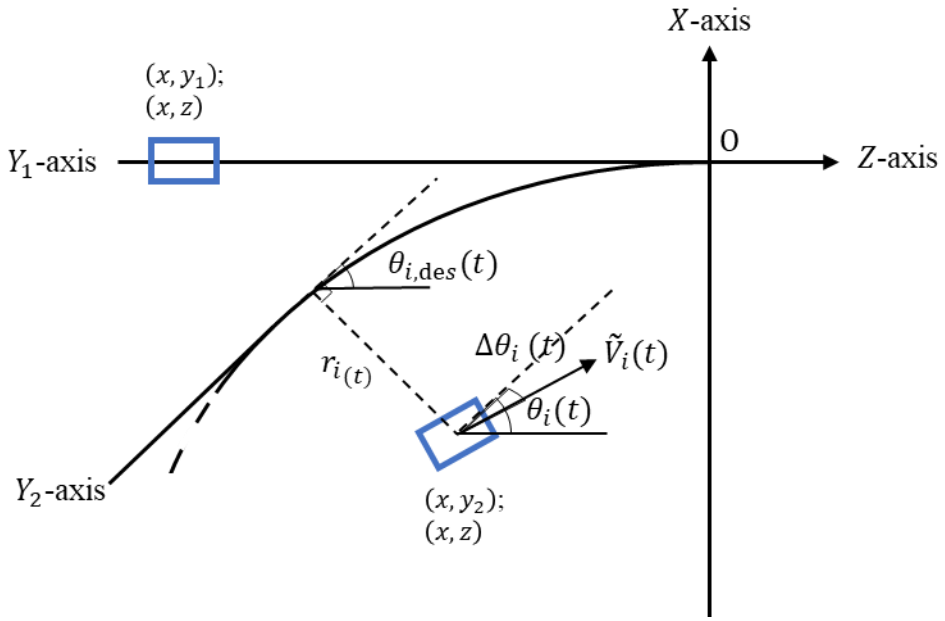

FIG. 3-4. Vehicle Dynamics in Path Coordinates Model

3.3.2 Holonomic Vehicle Lateral Dynamics

Then, the vehicle dynamics can be described by the state space as below:

$$\frac{dM_i(t)}{dt} = \frac{d}{dt}\begin{bmatrix} x_i(t) \\ r_i(t) \\ \Delta\theta_i(t) \end{bmatrix} = \begin{bmatrix} \tilde{v}_i(t) * \cos\left(\Delta\theta_i(t)\right) \\ \tilde{v}_i(t) * \sin\left(\Delta\theta_i(t)\right) \\ \mu_i(t) - \dfrac{\tilde{v}_i(t) * \cos\left(\Delta\theta_i(t)\right)}{R} \end{bmatrix}, \tag{45}$$

where $\tilde{v}_i(t)$ is the velocity of the CAV in the curvilinear coordinate. To make the structure and stability given by the longitudinal controller mentioned above still hold, we can simply let $v_i(t) = \tilde{v}_i(t) * \cos\left(\Delta\theta_i(t)\right)$, and the string stability refers to a projected practically string stability by $\cos\left(\Delta\theta_i(t)\right)$. $\mu_i(t)$ is the angular velocity of the CAV and R is the radius of the curvature. Note that, $x_i(t)$ is more related to the system level stability (string stability in our case), while the lateral movement is more related to the individual vehicle stability (usually known as local stability). Hence, for this extension of lateral control, we only need to consider the components of lateral deviation function $dr_i(t)/dt$ and angular deviation function $d\Delta\theta_i(t)/dt$ in Eq. (45). Therefore, we can define the lateral state $M_{i,l}(t)$ as $[r_i(t), \Delta\theta_i(t)]^T$, and the state space function for the lateral vehicle dynamics becomes:

$$\frac{dM_{i,l}(t)}{dt} = \frac{d}{dt}\begin{bmatrix} r_i(t) \\ \Delta\theta_i(t) \end{bmatrix} = \begin{bmatrix} \tilde{v}_i(t) * \sin(\Delta\theta_i(t)) \\ \mu_i(t) - \dfrac{\tilde{v}_i(t) * \cos(\Delta\theta_i(t))}{R} \end{bmatrix}. \tag{46}$$

However, the function is still complex because of nonlinearities caused by sine/cosine function. Luckily, the angle $\Delta\theta_i(t)$ is usually small enough (e.g., $\Delta\theta_i(t) < 14^{\circ}$, which also suggests $v_i(t) \approx \tilde{v}_i(t)$) that satisfy the small-angle approximation to simplify vehicle lateral dynamic which given as follow:

$$\frac{dM_{i,l}(t)}{dt} = \frac{d}{dt}\begin{bmatrix} r_i(t) \\ \Delta\theta_i(t) \end{bmatrix} = \begin{bmatrix} \tilde{v}_i(t) * \sin(\Delta\theta_i(t)) \\ \mu_i(t) - \dfrac{\tilde{v}_i(t) * \cos(\Delta\theta_i(t))}{R} \end{bmatrix}. \tag{47}$$

By defining $\mu_i(t)$ as the system control input, Eq. (47) can be expressed as a linear time variant system (LTV) as:

$$\frac{dM_{i,l}(t)}{dt} = \mathrm{A}_i(t) * M_{i.l}(t) + \mathrm{B}_i(t)\mu_i(t) + \mathrm{D}_i(t), \tag{48}$$

where $\mathrm{A}_i(t) = \begin{bmatrix} 0 & \tilde{v}_i(t) \\ 0 & 0 \end{bmatrix}$, $\mathrm{B}_i(t) = \begin{bmatrix} 0 \\ 1 \end{bmatrix}$, $\mathrm{D}_i(t) = \begin{bmatrix} 0 \\ -\frac{\tilde{v}_i(t)}{R} \end{bmatrix}$.

To determine the $\mu_i(t)$, we apply a widely applied ELQR by Singh & Pal, (2017) at each time point t in a rolling horizon manner according to the most recent measurement $\tilde{v}_i(t)$, which can be represented as:

$$\min J_i(M_{i,l}(t), \mu_i(t)) = \int_0^{\infty} M_{i,l}(t)^T Q M_{i,l}(t) + R\mu_i(t)^2 dt, \tag{49a}$$

$s.t.$

$$\frac{dM_{i,l}(t)}{dt} = \mathrm{A}_i(t) * M_{i,l}(t) + \mathrm{B}_i(t)\mu_i(t) + \mathrm{D}_i(t). \tag{49b}$$

Eq. (49a) is used to regulate the lateral and angular deviation of the state, and meanwhile consider the lateral control efficiency. Specifically, $M_{i,l}(t)^T Q M_{i,l}(t)$ determines the lateral control efficiency,

$R\mu_i(t)^2$ determines the lateral comfort, and $Q = \begin{bmatrix} \pi_1 & \\ & \pi_2 \end{bmatrix}$, $R = \pi_3$ are the pre-define diagonal positive-definite weighting matrices to guarantee the smoothness of the turning angular speed.

By solving the continuous ELQR, the optimal control for the lateral dynamic controller in Eq. (48) is given as a linear feedback and feedforward controller as below:

$$\mu_i(t) = k_{bi}(t)^T M_{i,l}(t) + k_{fi}(t) D_i(t). \tag{49c}$$

where $k_{bi}(t) = [k_{ri}(t), k_{\Delta\theta i}(t)]$ is the constant continuous feedback gain for the lateral deviation and angular deviation of vehicle i at time t, respectively, which can be solved by Continuous Algebraic Recatti Equation (Anderson & Moore, 2007) as below:

$$k_{bi}(t) = -{R_i}^{-1} B_i(t)^T P_i(t), \tag{50a}$$

$$k_{fi}(t) = -{R_i}^{-1} {B_i}^T(t) \left[\left(A_i - {R_i}^{-1} B_i(t) {B_i}^T(t) P_i(t) \right)^T \right]^{-1} P_i(t), \tag{50b}$$

$$P_i(t) A_i(t) + {A_i}^T(t) P_i(t) - P_i(t) B_i(t) {R_i}^{-1} {B_i}^T(t) P_i(t) = Q. \tag{50c}$$

3.3.3 Nonholonomic Vehicle Lateral Dynamics

To make the system more realistic, a nonholonomic vehicle dynamics system has been considered as an extension. The main difference from the holonomic system is taking the steering angle into account (Necsulescu et al., 2010). As shown in **FIG. 3-5**, the revised vehicle lateral dynamics state $\mathcal{M}_i(t)$ can be defined as $\mathcal{M}_i(t) = [r_i(t), \Delta\theta_i(t), \delta_i(t)]^T$ where the $\delta_i(t)$ denotes the steering angle of the vehicle, L_r denotes the spacing between the front and rear wheel.

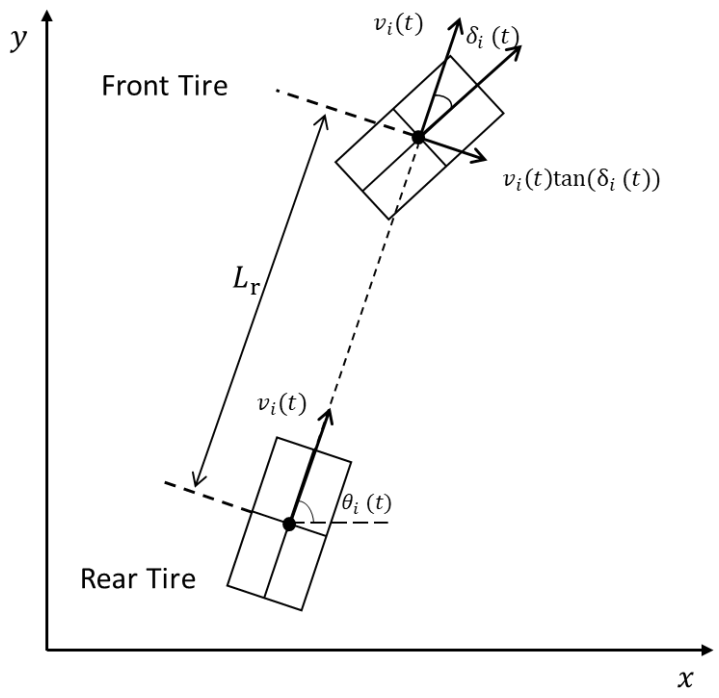

FIG. 3-5. Nonholonomic Vehicle Dynamics in Cartesian Coordinates Model

Then, the vehicle dynamics can be described by the state space as below:

$$\frac{d\mathcal{M}_i(t)}{dt} = \begin{pmatrix} v_i(t)\left(1-\frac{r_i(t)}{R_i(t)}\right)\tan(\Delta\theta_i(t)) \\ \frac{v_i(t)\left(1-\frac{r_i(t)}{R_i(t)}\right)\tan(\delta_i(t))}{cos(\Delta\theta_i(t))L_r} - \frac{v_i(t)}{R_i(t)} \\ \kappa_i(t) \end{pmatrix}, \tag{51}$$

where $R_i(t)$ denotes the radius of CAV i at time t for the nonholonomic system. $\kappa_i(t)$, which is the control input, represents the steering angular velocity of CAV i. Similar to Eq. (46), we apply a small-angle approximation for $\Delta\theta_i(t)$, which gives:

$$\frac{d\mathcal{M}_i(t)}{dt} = \begin{pmatrix} v_i(t)\left(1-\frac{r_i(t)}{R_i(t)}\right)\Delta\theta_i(t) \\ \frac{v_i(t)\left(1-\frac{r_i(t)}{R_i(t)}\right)\tan(\delta_i(t))}{L_r} - \frac{v_i(t)}{R_i(t)} \\ \kappa_i(t) \end{pmatrix}. \tag{52}$$

As can be found that, Eq. (52) still has a non-linear term, $\tan(\delta_i(t))$, where practically $\delta_i(t)$ is not small enough to make the small-angular approximation hold. Thus, to handle the non-linear continuous optimal control problem, a discretization step and a linearization step are usually applied. For discretization, the Forward Euler method (Puwal & Roth, 2007) is adopted, which transfer Eq. (52) to the Eq. (53) below:

$$\mathcal{M}_{i,t+t_s} = y_{i,t} + f\left(\mathcal{M}_{i,t}, u_{i,t}\right)t_s, \tag{53}$$

where t_s is the time discretization length (i.e. 0.001 sec in our case). Note that the equilibrium of the state space is $\mathcal{M}_e = [0,0,0]^T$, with $u_e = 0$. Then, by the first order Taylor series expansion, we can get the discretized LTV system:

$$\begin{aligned}\mathcal{M}_{i,t+t_s} \approx \mathcal{M}_{i,t} + \nabla f_{\mathcal{M}}(\mathcal{M},u)t_s|_{\mathcal{M}_{i,t}=\mathcal{M}_e}\left(\mathcal{M}_{\mathrm{i,t}} - \mathcal{M}_e\right) \\ + \nabla f_u(\mathcal{M},u)t_s|_{u_{i,t}=u_e}\left(\kappa_{\mathrm{i,t}} - u_e\right),\end{aligned} \tag{54a}$$

which can be further simplified as:

$$\mathcal{M}_{i,t+t_s} \approx \left(I + \nabla f(\mathcal{M},u)t_s|_{\mathcal{M}_{i,t}=\mathcal{M}_e}\right)\mathcal{M}_{i,t} + \nabla f_u(\mathcal{M},u)t_s|_{u_{i,t}=u_e} + D_{i,t}\frac{v_{i,t}}{R_i(t)}, \tag{54b}$$

where $\nabla f(\mathcal{M},u)t_s|_{\mathcal{M}_{i,t}=\mathcal{M}_e} = \begin{pmatrix} 0 & v_i(t)t_s & 0 \\ 0 & 0 & \frac{v_i(t)}{L_r}t_s \\ 0 & 0 & 0 \end{pmatrix}$, and $\nabla f_u(\mathcal{M},u)t_s|_{u_{i,t}=u_e} = \begin{pmatrix} 0 \\ 0 \\ t_s \end{pmatrix}$, $D_{i,t} = \begin{pmatrix} 0 \\ -t_s \\ 0 \end{pmatrix}$.

After simplification, the nonlinear system given in Eq. (54b) can be approximated as an LTV system:

$$\mathcal{M}_{i,t+t_s} \approx A^*_{i,t} \times \mathcal{M}_{i,t+t_s} + B^*_{i,t}\kappa_{i,t} + D^*_{i,t}\frac{v_{i,t}}{R_{i,t}}, \tag{55}$$

where $A_{i,t}^* = \begin{pmatrix} 1 & v_i(t)t_s & 0 \\ 0 & 1 & \frac{v_i(t)}{L_r}t_s \\ 0 & 0 & 1 \end{pmatrix}$, $B_{i,t}^* = \begin{pmatrix} 0 \\ 0 \\ t_s \end{pmatrix}$.

By modifying lateral state-space formulation, we can still apply a discrete version of ELQR controller in a rolling horizon fashion.

$$\min J_i(\mathcal{M}_{i,t}, \mu_{i,t}) = \sum_{t=0}^{\infty} {\mathcal{M}_{i,t}}^T Q \mathcal{M}_{i,t} + R{\kappa_{i,t}}^2, \tag{56a}$$

$s.t.$

$$\mathcal{M}_{i,t+t_s} \approx A_{i,t}^* \times \mathcal{M}_{i,t} + B_{i,t}^* \kappa_{i,t} + D_{i,t}^* \frac{v_{i,t}}{R_{i,t}}, \tag{56b}$$

where Q and R are the positive definite weighting matrix for system state and control input. By solving the above discrete ELQR, we can get the control law for the lateral movement as discrete linear feedback and feedforward controller given below:

$$\mathcal{M}_{i,t+t_s} \approx A_{i,t}^* \times \mathcal{M}_{i,t+t_s} + B_{i,t}^* \kappa_{i,t} + D_{i,t}^* \frac{v_{i,t}}{R_{i,t}}, \tag{57a}$$

where k_{fb}, and k_{ff} are linear feedback and feedforward gains solved by Discrete Algebraic Recatti Equation (Lancaster & Rodman, 1995) as below:

$$k_{fb} = -\left(R + {B_{i,t}^*}^T {P_{i,t}}^* B_{i,t}^*\right)^{-1} {B_{i,t}^*}^T P_{i,t}^* A_{i,t}^*, \tag{57b}$$

$$\mathrm{k_{ff}} = -\left(R + {B_{i,t}^*}^T {P_{i,t}}^* B_{i,t}^*\right)^{-1} {B_{i,t}^*}^T P_{i,t}^* A_{i,t}^* \left(A_{i,t}^* - {P_{i,t}^*}^{-1}\left(P_{i,t}^* - Q\right)\right)^{-1} D_{i,t}^*, \tag{57c}$$

$$P_{i,t}^* = Q + A_{i,t}^* \left[P_{i,t}^* - P_{i,t}^* B_{i,t}^* \left(R + {B_{i,t}^*}^T {P_{i,t}}^* B_{i,t}^*\right)^{-1} {B_{i,t}^*}^T {P_{i,t}}^*\right] A_{i,t}^*. \tag{57d}$$

Remark 2. For a lane change problem or a parallel ramp layout, we can treat the designed trajectory curve as any generic twice-differentiable curve (Υ) on a plane by a consecutive (x, y) points in a global Cartesian Coordinate. By the construction of curvilinear coordinate, the differentiable curve can be parametrized as $\Upsilon(s) = \left(p_x(s), p_y(s)\right)$ (Sendra & Winkler, 1991), where $p_x(s)$ and $p_y(s)$ are the

global Cartesian Coordinate over the point s on the curve. By the road intelligence, the corresponding curve radius at each point s can be pre-calculated as the reciprocal of the curvature $\mathrm{K}(s)$ as below:

$$R(s) = \frac{1}{\mathrm{K}(s)} = \frac{1}{\sqrt{\left(\frac{d^2 p_x(s)}{ds^2}\right)^2 + \left(\frac{d^2 p_y(s)}{ds^2}\right)^2}}. \tag{58}$$

During vehicle operation, since the controller is implemented in a rolling horizon, at each time point t, we can update the corresponding value $\mathrm{R(t)}$ based on current vehicles position s, to implement the ELQR control.

4. NUMERICAL SIMULATION RESULT FOR MODELLING

This chapter presents numerical simulations to validate the efficiency and stability of our proposed control strategy. Both equally weighted and non-equally weighted information cases mentioned above are conducted on MATLAB. Since we design the longitudinal controller as a system-based controller and the lateral controller as a local-based controller, the experimental analysis of these two are discussed separately.

4.1 Simulation of Longitudinal Controller

Firstly, to validate the correctness and effectiveness of the proposed propositions, we set the range of the desired time gap at $\tau = [0.5,1,1.5]$ and the number of communicated predecessors $N_i \in [1,6]$ in order to find the feasible region of control gains for two cases. Based on these settings and the propositions, the results shown in **FIG. 4-1**. illustrate that the boundaries of the relationship between ω_e and ω_v is proportional, and with the number of CAVs in the communication topology (N_i) increases, the eligible combination of weight coefficients (the area under the boundaries) increases, which indicates that the longitudinal controller we designed is practical. Additionally, this growth trend is reflected in a desired time gap of vehicle, τ. As τ increases, the area under the boundaries increases. Specifically, though two cases follow the same trends, the equally weighted case shown in **FIG. 4-1** (a)-(c) has more eligible combinations of the weight coefficients than the non-equal weighted ones shown in **FIG. 4-1** (d)-(f).

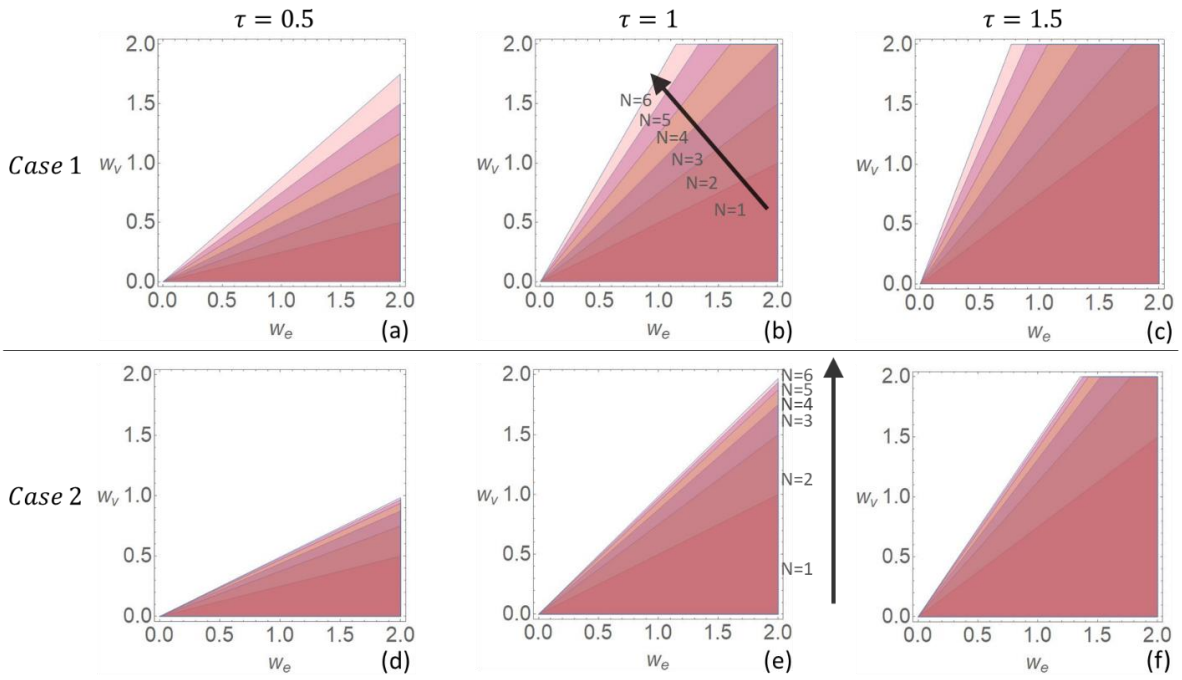

FIG. 4-1. Feasible region of control gains for string stability (a)-(c) Equally weighted case, (d)-(f) Non-equally weighted case

Given control gain analysis, the default parameter values for the CAVs controller design are shown as **Table. 4-1** to conduct CAVs trajectories simulation. The experiment setup consists of 12 CAVs control simulation with one leading vehicle. Since the vehicle initial speed is set to 20 m/s, to better reflect our algorithm, we preset the average distance between two adjacent cars to 20 meters with random $[-10,10]$ meters deviation. Based on that, the origin locations of the CAVs are randomly generated. In this example, the 12 CAVs are initially set up as 7 vehicles on mainline and 5 vehicles on on-ramp whose corresponding relative distance to the merging point are $P_M = [0, -30, -46, -68, -89, -165, -186]$ and $P_R = [-20, -109, -132, -154, -198]$. By applying the virtual car sequencing method, the initial positions of 12 CAVs on the virtual Z-axis are determined by Eq. (2) above as $P_z = [0, -20, -30, -46, -68, -89, -109, -132, -154, -165, -186, -198]$ as shown in **FIG 4-2**. Meanwhile, the movement of the leading vehicle is generated based on a sine velocity function which indicates the back-and-forth changes of the velocity in a short amount of time

that can directly reflect the optimization result of the control algorithm. The mean value of the sine function is set to the initial speed, the oscillation magnitude is set to 3 and the frequency is set to 0.0005 to better visualize the result. The merging point is set to 600 meters away from the first CAV entering the system. To make the simulation closer to the reality, the acceleration threshold is set to $[-3,3]\ m/s^2$. Note that both cases use the exactly identical control parameters mentioned in Table 1. **FIG. 4-3** below shows the state evolution of a) position of the 12 CAVs on virtual Z-axis, b) the speed, c) the acceleration and d) the position of CAVs on the mainline (Y_1-axis) for the equally weighted information case.

Table 4-1. Default value setting for the longitudinal controller experimental design.

Parameters	Value
Time Discretization Rate t_s	0.001
Total Running Time T	80 sec
τ	1 sec
L	5 m
$v_{initial}$	20 m/s
ω_e	1.4
ω_v	0.3

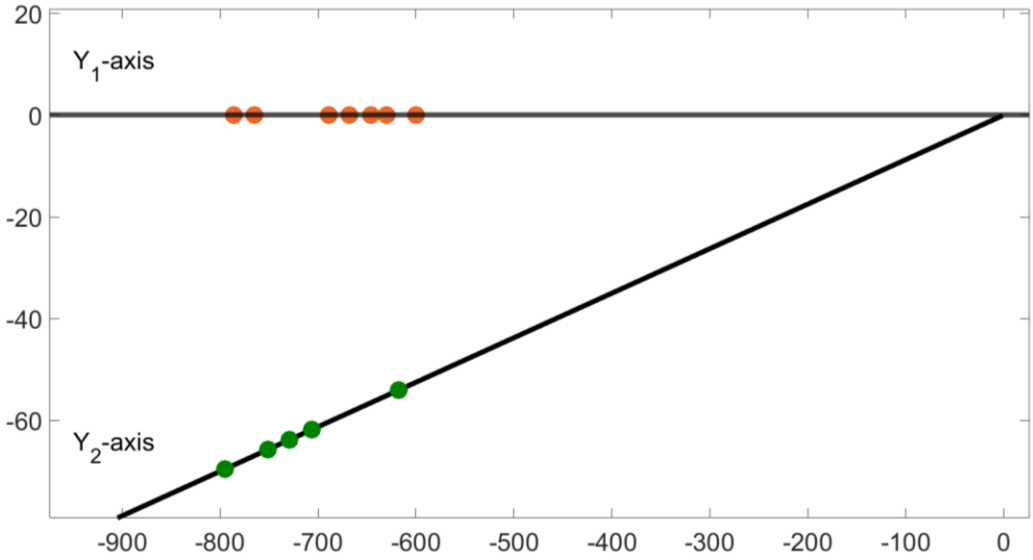

FIG. 4-2. The initial position of 12 CAVs on y_1 and y_2 axis.

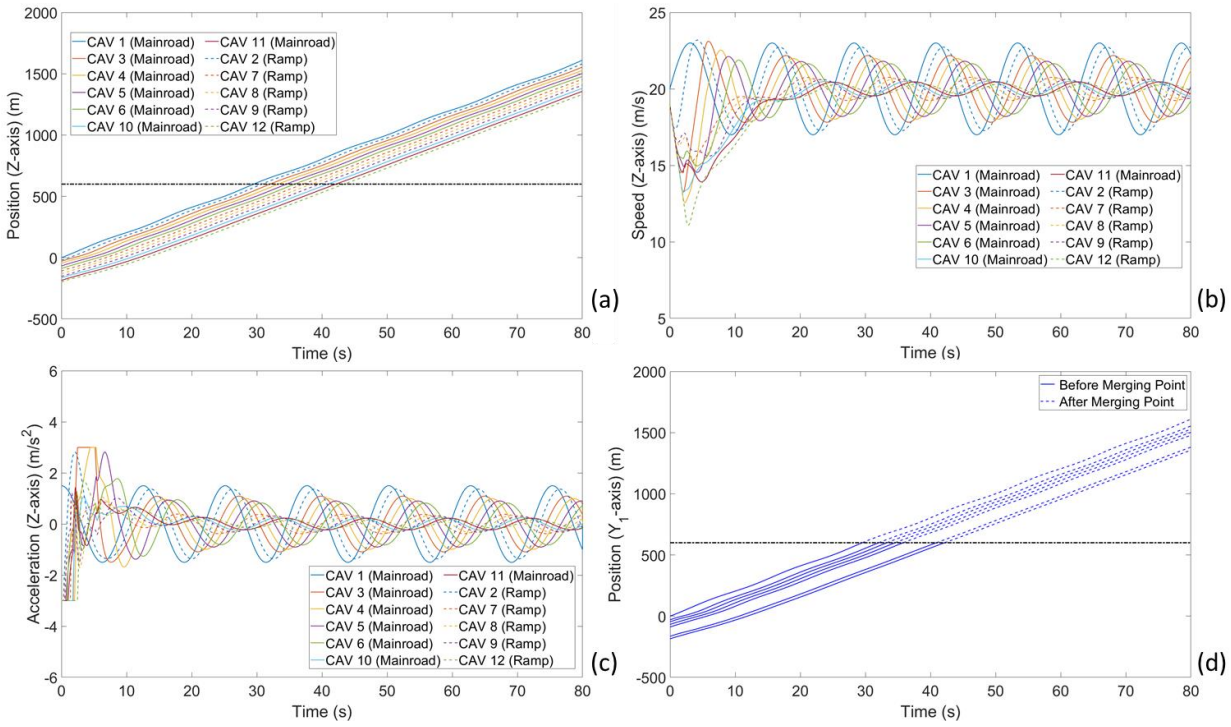

FIG. 4-3. State evolution results of longitudinal controller for Case 1: (a) Platoon Position on Z-axis (b) Speed (c) Acceleration (d) Platoon Position on Y_1-axis

Similarly, **FIG. 4-4** shows all the result for Case 2, which is a non-equally weighted information case.

It is observed that the disturbances are dampened along the string of CAVs in both state of speed and acceleration. Additionally, the state of position for CAVs on virtual Z-axis and real-world mainline Y_1-axis are well reflected the shrink trend. Thus, this trend illustrates that not only the CAVs on the mainline and on the on-ramp are string stable, but also the mapped virtual platoon on the virtual Z-axis is string stable. Meanwhile, the state of the position results also demonstrates that CAVs are controlled stably in the set time gap to ensure safety. Further, the result validates the proposed controller can actively reduce the voids in a small amount of time and meanwhile guarantee the string stability of the whole system in both cases.

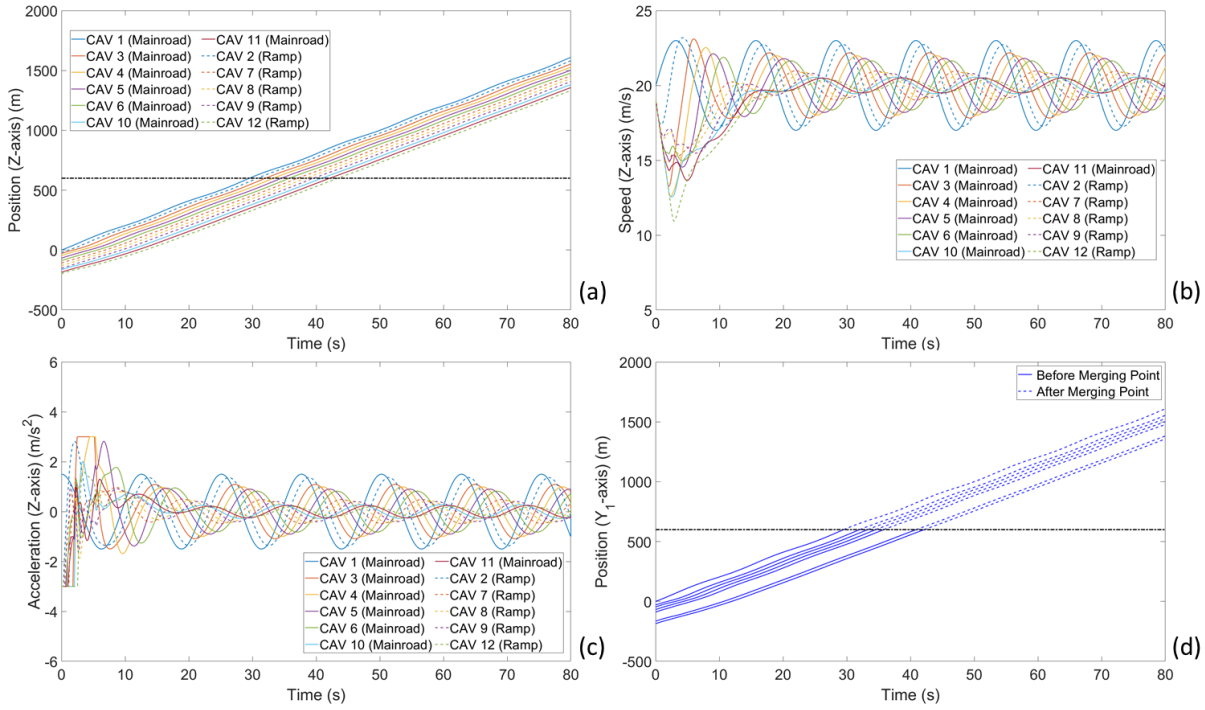

FIG. 4-4. State evolution results of longitudinal controller for Case 2: (a) Platoon Position on Z-axis (b) Speed (c) Acceleration (d) Platoon Position on Y_1-axis

To more quantitatively validate the proposed longitudinal controller that satisfy the propositions mentioned in **Chapter 3**, we use the square of L_2 norm of the absolute velocity for each CAV to verify. **FIG. 4-5** shows the result of the square of L_2 norm of the absolute velocity (energy) for case 1 and 2. The trends for both cases elucidate that the energy is attenuated through the control of vehicles.

Specifically, this attenuation trend applies to CAVs on Y_1-axis (red bars), on Y_2-axis (blue bars), and on the virtual Z-axis. Thus, the results validate the string stability criterion we proposed in **Chapter 3.2**.

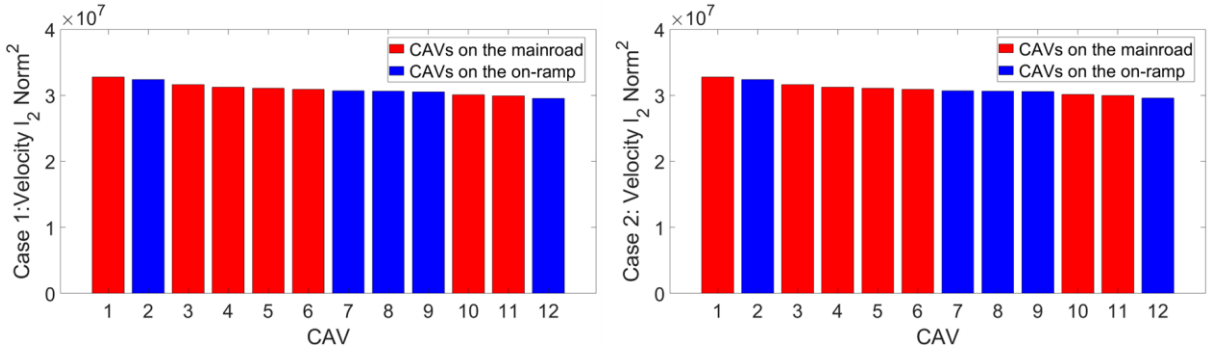

FIG. 4-5. Square of l_2 norm of absolute velocity comparison for case 1 and case 2.

4.2 Sensitivity Analysis for Longitudinal Controller

To examine whether merging control range is ample enough before merging, a numerical sensitivity analysis has been designed for the proposed longitudinal controller. Specifically, an extreme case has been conducted to find the minimum control range that allows CAVs on the virtual axle approach to equilibrium state before merging. In this experiment, the extreme case consists of 4 CAVs, 2 on mainline and 2 on on-ramp, where the initial positions of the CAVs on the virtual Z-axis violates the safety constraint (smaller or equal to the time gap). Meanwhile the leading vehicle is designed to brake sharply in a short amount of time during the simulation to test the resilience of the proposed controller. For consistency, the experiment follows the default settings in **Table 4-1** but with 40 seconds simulation time. The initial positions of CAVs on the mainline are $X_M = [0, -8]$, and the initial positions of CAVs on the on-ramp are $X_R = [-2, -9]$. By applying the virtual car sequencing method, the initial position of 4-CAV platoon on the virtual axle are $X_Z = [0, -2, -8, -9]$. The leading vehicle is set to decelerate at 2 ms^{-2} after running for 13 sec until the velocity reach $10ms^{-1}$, then accelerate again at 2 ms^{-2} after running for 26 sec until reach the initial velocity, $20ms^{-1}$. Note that, since the mainline/ramp indicator set $\tilde{F}_z = [1,0,1,0]$, the weighted coefficients are equal in both equally weighted and non-

equally weighted case. Thus, we only apply the equally weighted case string stability criterion in this analysis. **FIG. 4-6** illustrates the 4 CAVs' state evolution of a) position on Z-axis, b) deviation of the target spacing, and c) the square of l_2 norm of absolute velocity of the 4 CAVs.

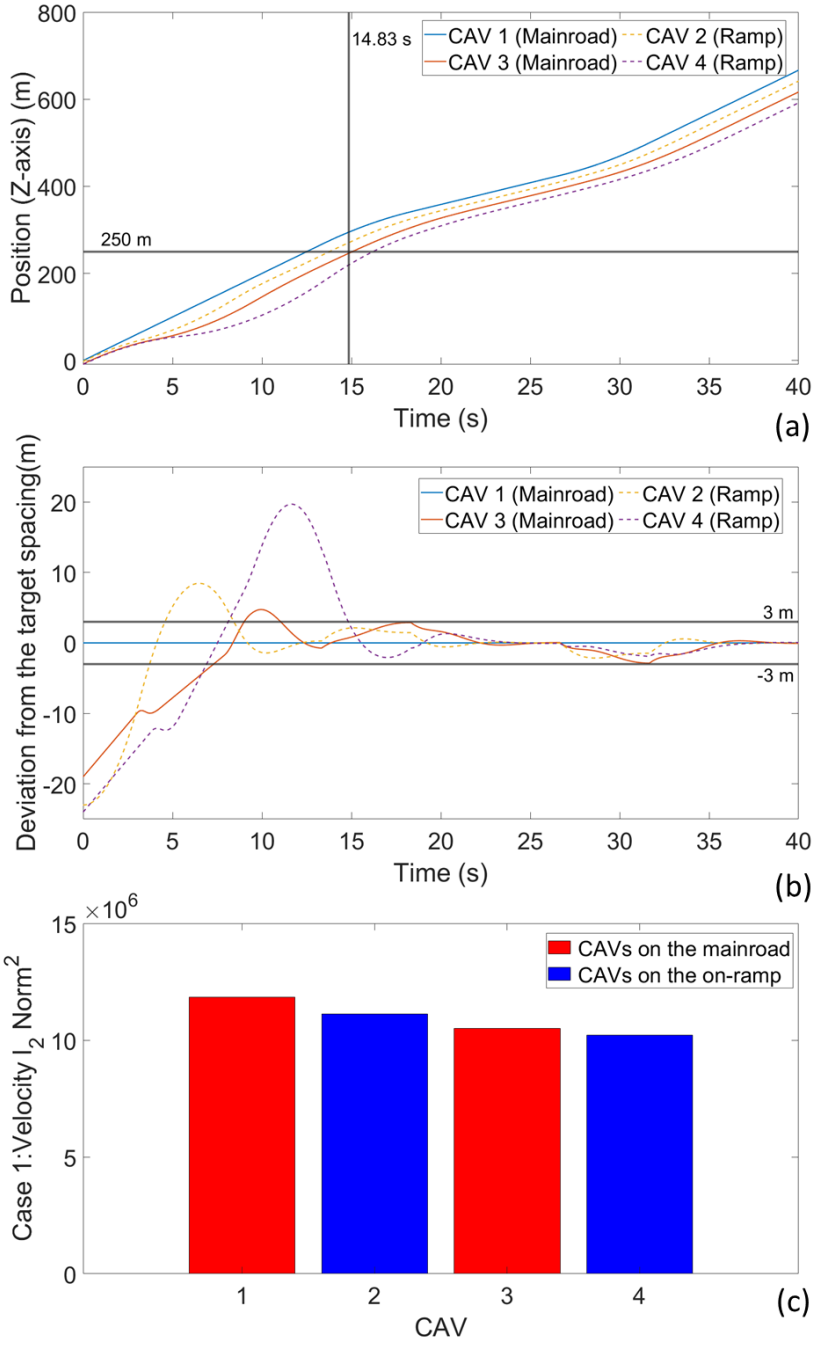

FIG. 4-6. Sensitivity analysis result: (a) Platoon Position on Z-axis (b) Deviation from the target spacing (c) Square of l_2 norm of absolute velocity.

Deviation from target spacing (i.e., $x_{i-1}(t) - x_i(t) - d_{i,1}(t)$) has been used to verify whether the CAVs reach equilibrium close enough for merging CAVs. Specifically, in this case, we define that when the deviation from target spacing meets the range $[-3,3]$, the corresponding CAV get close to equilibrium and can merge to the mainline relatively safely. In **FIG. 4-6** (b), it is observed that, until the fourth CAV drive for 14.83 sec, the whole platoon on the virtual axle meets the range $[-3,3]$ which close enough to the equilibrium state and the corresponding travelling distance is around 220 m. Thus, we can conclude that the assumption we made in **Chapter 1** is ample enough for the purposed controller.

4.3 Simulation of Lateral Controller

Next, we evaluate the extended lateral controller by another numerical experiment. Since we design the lateral controller as a local controller, each CAV is controlled individually, the experiment is designed to focus on one of the CAVs in the platoon. As mentioned in **Chapter 3.3**, the lateral movement is more related to the individual vehicle stability, thus we determine the state evolution of lateral deviation and angular deviation to validate the effectiveness of the lateral controller. The parameter settings are given in **Table 4-2** as an example. Note the initial angular deviation is set to 10° to satisfy small-angle approximation. In this experiment, we select #2 CAV in the platoon, the first CAV entering the on-ramp lane, as the test subject. Since the initial position of the test CAV is located at -620 meter on Y_2-axis, the θ_{des} can be calculated as 36°. **FIG. 4-6** demonstrates the schematic diagram of the lateral experiment in a real-world scene.

Table 4-2. Default value setting for the lateral controller experimental design.

Parameters	Value
Initial lateral deviation	0.4
Initial angular deviation	-10°
Radius of the on-ramp	1000 m
T	80 sec

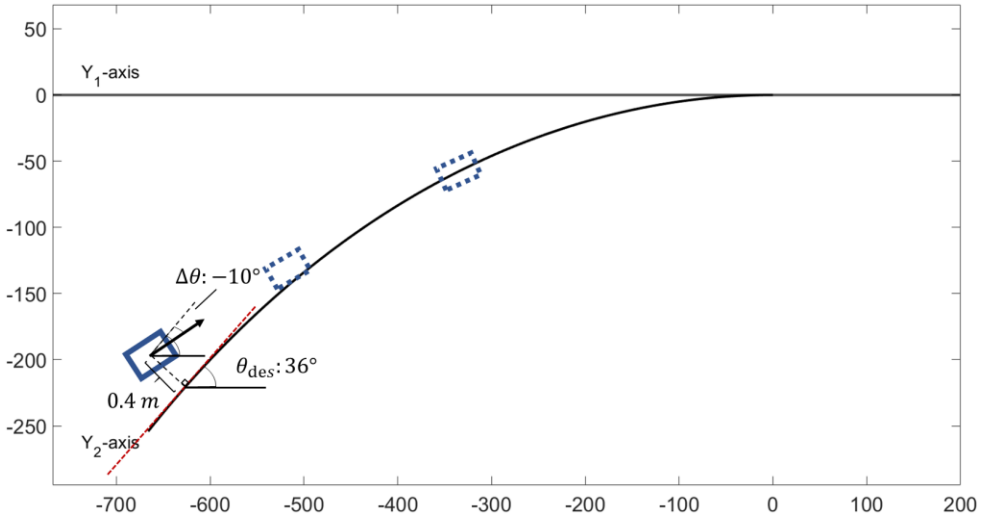

FIG. 4-7. Schematic diagram of lateral experiment in real-world scene

The evaluation of the holonomic system is based on two results: 1) the state evolution of lateral deviation and 2) angular deviation for the first on-ramp vehicle as shown in **FIG. 4-7** (a), (b), since other on-ramp vehicles also exhibit the same conclusion. The result illustrates that the CAV controlled by the lateral controller converges to the road's centerline (infinitely close to 0) very quickly. However, it is observed that, at the time 32 sec, both deviations have a slight peak of changes (disturbances) which indicates that the CAV is passing through the merging point. Due to the small amount of change and instant amount of time, the changes can be neglected.

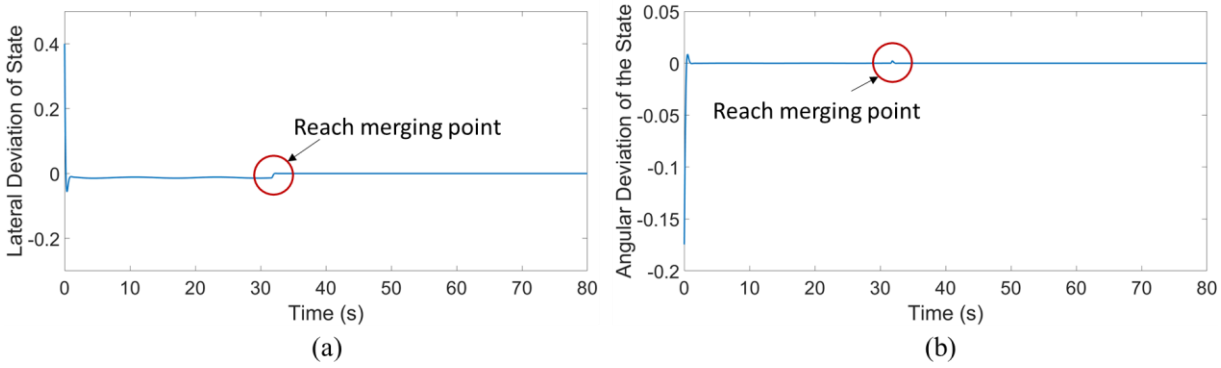

FIG. 4-8. Holonomic system results: state evolution of (a) lateral deviation and (b) angular deviation.

The evaluation of the nonholonomic lateral controller has a corresponding steering angle validation

term besides lateral and angular deviation. The initial steering angle of the testing CAV is set to 0. Similar trends have been observed in the results shown in **FIG. 4-9**. Not only the lateral and angular deviation converge fast, but the vehicle steering angle also quickly converges to the designed road steering angle at the same time. Note that, after the vehicle merging to the mainline, the steering angle continuously to be infinitely close to 0 indicates that the vehicle is driving along a straight line. Overall, both holonomic and nonholonomic results well-reflect the control efficiency and smoothness of the lateral movement.

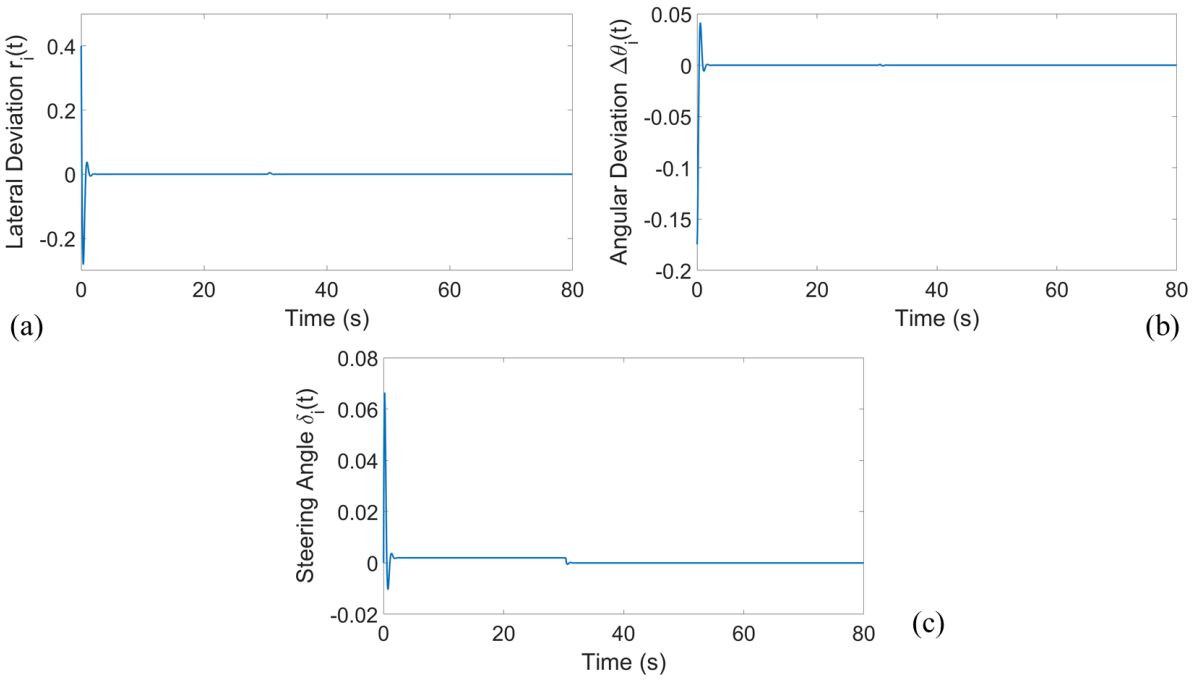

FIG. 4-9. Nonholonomic system results: state evolution of (a) lateral deviation, (b) angular deviation, and (c) steering angle.

5. STOCHASTIC CAV CAPACITY ANALYSIS

Based on the finding gaps in literature reviews, we want to design a unified framework incorporating multiple high-dimensional factors to understand the parametric impact on stochastic capacity under on-ramp merging scenario. The high-dimensional factors comprise of both macroscopic characteristics such as vehicle's communication capability and corresponding topology, and microscopic characteristics such as vehicle control gains. To step-by-step clarify the above objective, we first extend the string stability criterion designed above to illustrate the relationship between the desired time gap and other parameters of the CAV control strategy. Then to fit the stochasticity of communication loss, we exploit a stochastic capacity model in a generic CAV CF scene. Further, we extend the CF capacity model to a merging capacity model by adding one more stochastic feature, vehicle arrival pattern.

5.1 Microscopic Controller Extension

Recall that in **Chapter 3.3**, a string stability criterion has been applied to ensure traffic oscillation attenuation of the control system. Particularly, the sufficient string stable condition is a function with respect of control gains ω_e and ω_v, the desired time gap τ, and number of communicated predecessors N_i. By transferring the condition into a τ function we can have:

$$\tau \geq \frac{4\omega_v}{\omega_e(1+N_i)}. \tag{59}$$

Then, based on the relationship among the parameters in Eq. (59), the minimum τ can be calculated if the boundary of equilibrium velocity difference is minimum and boundary of equilibrium spacing error is maximum as follow:

$$\tau_{min}(N_i) = \max\left(\tau_{safe}, \frac{4\omega_{v,min}}{\omega_{e,max}(1+N_i)}\right), \tag{60}$$

where τ_{safe} is a predefined value for τ for safety concerns.

Note that, only the equal relationship in Eq. (59) has been retained when we express the τ_{min}. Since, by definition, the capacity is the inverse of τ, we want to use τ_{min} to find the maximum sustainable flow rate of the road. Therefore, values greater than minimum are not considered in the following study.

5.2 Capacity Modelling for Car-following Scenario

In this session, we determine a capacity estimation model for CAV CF scenario based on vehicles' stochastic communication capabilities. We firstly give a generic stochastic capacity model including expected capacity and variance based on an assuming probability mass function (PMF) of a vehicle communication capability function. Then, we provide a detailed PMF example by using a Signa-Interface-plus-Noise-Ratio (SINR) (Du & Dao, 2014) as a special case.

To make capacity analysis easier to understand, we mainly address the analysis into two parts, from relatively simple CF capacity modeling to more complex on-ramp merging capacity modeling. Based on the literature reviews (Bian et al, 2019), we have found that vehicle communication capability is one of the main factors that affect the CAV CF control. Therefore, different from many research (Zhou & Ahn 2019; Duret et al., 2019) that assuming deterministic models for the communication failure while ignoring stochasticity of communication capability and to make the following macroscopic analysis closer to the reality, we have relaxed the "no communication delay or loss" assumption proposed in **Chapter 1.4**. That means the N_i in Eq. (60) no longer is a fixed value calculated by the MLT we designed, but a stochastic parameter affects by the communication loss. Therefore, we define a new stochastic parameter, $N_{i,cap}$, to represents the capability of each vehicle to receive information from its predecessors without communication loss. In other words, $N_{i,cap}$ denotes the number of continuous predecessors that vehicle i can communicate.

Then, the Eq. (60) can be rewritten as:

$$\tau_{min}(N_{i,cap}) = \max\left(\tau_{safe}, \frac{4\omega_{v,min}}{\omega_{e,max}(1+N_{i,cap})}\right). \tag{61}$$

Further, based on the definition, the corresponding capacity of the road segment can be calculated as the inverse of τ_{min} as follow:

$$C_{cf} = \frac{1}{\tau_{min}(N_{i,cap}) + \frac{L}{V_{free}}} = \frac{1}{\max\left(\tau_{safe}, \frac{4\omega_{v,min}}{\omega_{e,max}(1+N_{i,cap})}\right) + \frac{L}{V_{free}}}, \tag{62}$$

where C_{cf} represents the capacity determined in the CF scenario; V_{free} denotes the free flow speed of the road segment. Moreover, since $N_{i,cap}$ is directly related to the stochasticity of communication capability, we need to theoretically determine the expected (mean) capacity and variance among different probabilities of $N_{i,cap}$.

For a coherent understanding, lets first assume a known PMF of $N_{i,cap}$, and denote it as $\Pr(N_{i,cap})$. Then, the expected capacity, given the know stochasticity of $N_{i,cap}$ can be formulated as:

$$E[C_{cf}] = \frac{1}{\sum_{i=1}^{N_{max}}\left(\tau_{min}(N_{i,cap}) + \frac{L}{V_{free}}\right) * \Pr(N_{i,cap})} \tag{63}$$

$$= \frac{1}{\sum_{i=1}^{N_{max}}\left(\max\left(\tau_{safe}, \frac{4\omega_{v,min}}{\omega_{e,max}(1+N_{i,cap})}\right) + \frac{L}{V_{free}}\right) * \Pr(N_{i,cap})},$$

where N_{max} represents the maximum of vehicles within a communication range (e.g., N_{max} = 5 within 200 meters). Then, the corresponding variance can be formulated as:

$$Var(C_{cf}) = EC_{cf}^2 - (EC_{cf})^2 \tag{64}$$

$$= \frac{1}{\sum_{i=1}^{N_{max}} \left(\tau_{min}^2(N_{i,cap}) + \frac{L}{V_{free}}\right) * Pr(N_{i,cap})}$$

$$- \left(\frac{1}{\sum_{i=1}^{N_{max}} \left(\tau_{min}(N_{i,cap}) + \frac{L}{V_{free}}\right) * Pr(N_{i,cap})}\right)^2.$$

We have determined the general formulae for both expected capacity and variance of stochastic CF capacity model. Now we can get back to find out a way to calculate the stochasticity of $N_{i,cap}$.

5.2.1 Communication Loss Special Case based on SINR

In this study, we use SINR, one of the commonly used models in the wireless communication system (e.g., V2V) (Du & Dao, 2014), to simulate the stochasticity of communication loss since its measurement uses multiple realistic impact factors such as incoming signal power, interfering power and noise. In our case, we use it to measure the communication loss between vehicle and its predecessors. Specifically, by the definition, the SINR status $S_{i,i-k}^t$ between the receiver vehicle i and transmitter vehicle $i-k$ at time step t is specified as:

$$S_{i,i-k}^t = \frac{Q_{i-k,i}^t}{I_i^t + O}, \tag{65}$$

where $Q_{i-k,i}^t$ represents the power of the incoming transmitted signal from vehicle $i-k$ to i; I_i^t denotes the interference power from other signals to vehicle i, and O indicates the noise term. More detailed, $Q_{i-k,i}^t$ is defined as: $Q_{i-k,i}^t = P_{i-k}(X_{i-k,i}^t)^{-\alpha}$, where P_{i-k} denotes the transmission power of vehicle $i-k$; α is the signal power decay; $X_{i-k,i}^t$ represents the distance between two vehicles. Thus, $Q_{i-k,i}^t$ incorporates the transmission property that the transmit signal power will decay with the increase of the connection distance. Meanwhile, the interference term is defined as $I_i^t =$

$\sum_{m=1,m\neq k}^{N_{max}} e_{i-m}P_{i-m}\left(X_{i-m,i}^{t}\right)^{-\alpha}$, sums of the interference signal power from all other proceeding vehicles except vehicle $i-k$ in the communication range. e_{i-m} indicates the communication status where $e_{i-m}=1$ if proceeding vehicle $i-m$ is allowed to share and receive information; $e_{i-m}=0$ otherwise. Note that, for the noise term O, a normal distribution (e.g., $O\sim\mathcal{N}(\mu_O,\sigma_O^2)$) is adopted to illustrate the stochasticity of the noise effect. Hence, Eq. (65) can be further extended as:

$$S_{i,i-k}^{t}=\frac{P_{i-k}\left(X_{i-k,i}^{t}\right)^{-\alpha}}{\sum_{m=1,m\neq k}^{N_{max}} e_{i-m}P_{i-m}\left(X_{i-m,i}^{t}\right)^{-\alpha}+O}. \tag{66}$$

Then, we set a corresponding information transmission status $\eta_{i,i-k}^{t}$ to directly illustrate whether the information successfully transmit between vehicles based on $S_{i,i-k}^{t}$:

$$\eta_{i,i-k}^{t}=\begin{cases}1, if\ S_{i,i-k}^{t}>\beta\\ 0, if\ S_{i,i-k}^{t}\leq\beta\end{cases}, \tag{67}$$

where β is a threshold value determined by the communication modulation and code rate. To make it easier to understand, an intuitive example has been provided in **FIG 5-1**.

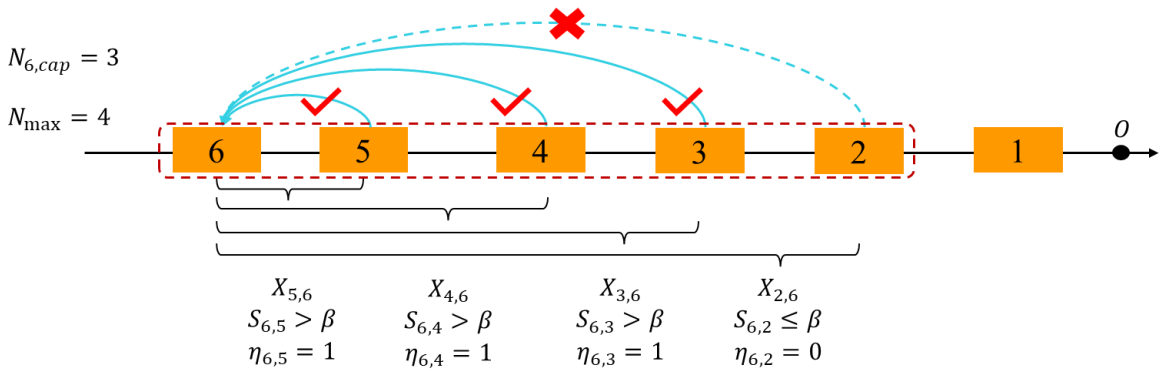

FIG. 5-1. An example of SINR status calculation

As the figure shows, since N_{max} is set to 4, for the CAV 6, it is allowed to communicate with CAV 5 to CAV 2. Then, based on the SINR status calculation, if $S_{6,5}$ is larger than the predefined threshold,

the $\eta_{6,5}$ is marked as 1 which means the CAV 6 can receive information from CAV 5. The same thing happened if $\eta_{6,4}$ and $\eta_{6,3}$ are marked as 1. However, if $\eta_{6,2}$ is marked as zero, even CAV 2 is within the communication range, no communication is allowed between the sixth CAV and second CAV. Thus, the $N_{6,cap}$ is determined as 3 in total.

Further, since currently there are no microscopic CAV empirical data to calculate the exact distance between each vehicle, a generic equilibrium state formula with an operation error term has been used to approximate the $X_{i-k,i}^{t}$ as follow:

$$X_{i-k,i}^{t} \approx k * \left(V_{free} * \ E[\tau] + L\right) + \sum_{1}^{k} Q_k, \tag{68}$$

where Q_k denotes the stochastic operation error for vehicle $i-k$ and it is adopted by a normal distribution (e.g., $O \sim \mathcal{N}(\mu_Q, \sigma_Q^2)$) to represent the stochasticity of Q_k in the following numerical simulation. Note that, we use the expected τ, $E[\tau]$, as one of the inputs to estimate the distance. Further, we can recalculate this expected τ by applying SINR to sampling the PMF of $N_{i,cap}$. And theoretically, the input τ should be equal to the output τ. Therefore, since $E[\tau]$ is not known, a specific algorithm has been designed to approximate the expected τ as close as possible to the reality. The detailed data flow of this algorithm is shown in **FIG 5-2**.

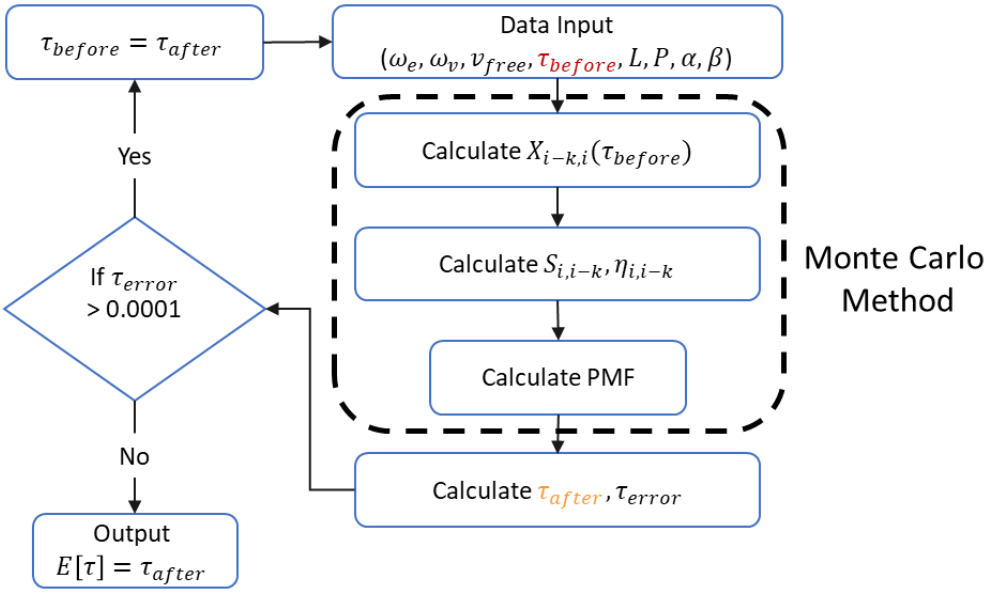

FIG. 5-2. Detailed data flow of the SINR sampling algorithm

The data input includes the initial τ as τ_{before}, control gains, initial velocity, and all the parameters in SINR calculation. Then, the corresponding $X_{i-k,i}^t$, $S_{i,i-k}^t$, and $\eta_{i,i-k}^t$ can be determined. By using the Monte Carlo method (Metropolis & Ulam, 1949) to sample the PMF of $N_{i,cap}$, the expected τ, τ_{after}, can be recalculated. Next, by comparing the difference between these two values, if the difference,τ_{error}, is smaller than a threshold (e.g., 0.0001), we conclude the τ_{after} is finalized and can be considered as the theoretically expected τ. Thus, by using this finalized τ, the corresponding expected capacity and variance can be determined based on Eq. (63) and (64).

5.3 Capacity Modelling for On-ramp Merging Scenario

Different from the above CF stochastic capacity model, not only communication capability will affect the capacity, but the random vehicle arrival pattern from mainline and on-ramp will also it. Thus, in this session, a new parameter, stochasticity of arrival pattern, has been introduced to formulate the on-ramp merging capacity model based on the CF model. Specifically, we use an exponential distribution to represent the vehicle arrival rate. One of the unique properties of exponential is the memoryless-ness,

which means each event occurs continuously and independently. Thus, the arrival of one vehicle won't affect the next arriving vehicle.

Although the virtual rotation concept in **Chapter 3** facilitates the conversion from CF capacity model to on-ramp capacity model, some definitions of the parameters need to be reorganized. Particularly, the definition of N_{max} remain the same as the maximum communication range for each vehicle. The definition of $N_{i,cap}$ has slightly different, it still represents the number of continuous predecessors that vehicle i can communicate but is limited to the MLT we designed. That means, if $N_{i,cap}$ is larger than the number of allowed communicated vehicles determined from MLT rules, we will still count all the probability of vehicles larger than the limit, but we only allowed vehicles that obey the MLT rules to communicate to vehicle i. Further to facilitate the following mathematic expression and understanding, we define k as the in-between vehicles in a communication subset and denotes as $k = [0,1, \dots, N_{i,cap} - 1]$.

Based on the definition of the exponential distribution, we first define the expectation (mean) arriving interval of CAVs on mainline and on-ramp at the merging point as μ_m and μ_r. And the corresponding arrival rate of mainline and on-ramp are defined as λ_m and λ_r as the inverse of arrival interval ($\frac{1}{\mu}$). Then, we further define an event E_k as any combination of MLT communication subsets with k number of in-between vehicles that pass through the merging point in a certain amount of time. And E_k happened is denoted as $E_k = 1$. **FIG. 5-3** shows all the combinations of E_k. Specifically, E_k has two forms as general event and special event. The general events illustrate the MLT subset with k number of in-between vehicles coming from the same lane, while the special event illustrates with 0 numbers of in-between vehicles. Moreover, the general events have two types whether the leading vehicle is from mainline or on-ramp and we denote these two as $L = m$ and $L = r$. Since the difference between these two types is the vehicle sequence, for the following mathematic proofs, only one of them is used for demonstration.

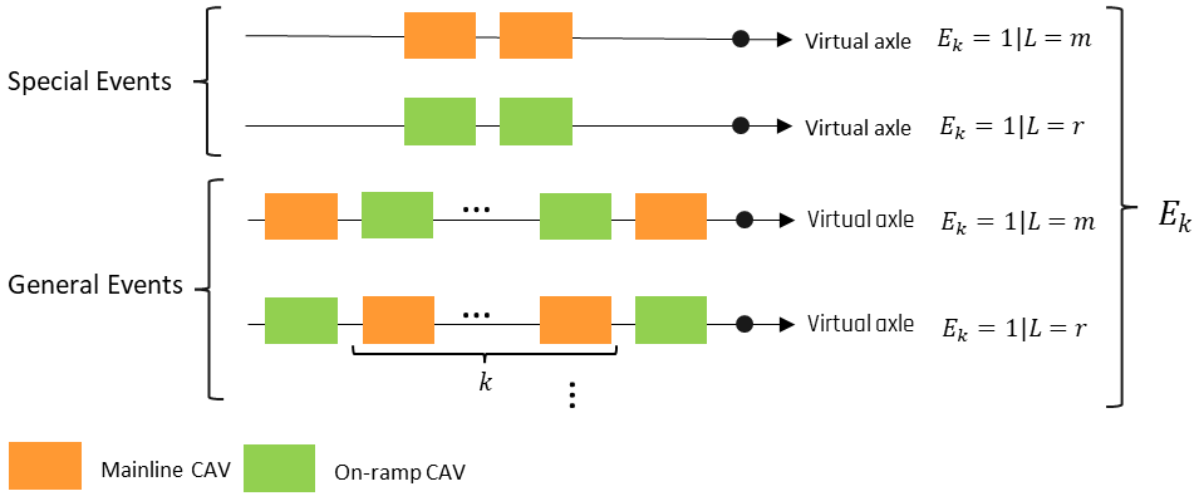

FIG. 5-3. Schematic diagram to illustrate all the combinations of E_k

5.3.1 Stochasticity of Arrival Pattern for On-ramp Capacity Model

We first begin with the probability determination for general events since the probability of special events can be determined as one minus the summation of all the probability of general events. Thus, based on the above definitions, proposition 4 can be formulated as:

Proposition 4. The conditional probability of E_k happened when the first and last CAVs in the topology subset is coming from the mainline follows:

$$\Pr(E_k = 1|L = m) = \left(\frac{\lambda_r}{\lambda_m + \lambda_r}\right)^k * \left(\frac{\lambda_m}{\lambda_m + \lambda_r}\right)^2, \forall k \in [0,1,\dots,N_{max} - 1], \tag{69}$$

where $E_k = 1$ means the event happened, 0 means the event did not happen. L determines the leading vehicle in the communication subset is from mainline (m) or on-ramp (r). And λ_r and λ_m are the arriving rate of the distribution for CAVs on on-ramp and mainline. Note that the k starts from zero which indicates no internal on-ramp vehicles between two adjacent mainline vehicles on the virtual axle. **FIG 5-4** shows the probability steps to facilitate the understanding of the following proofs.

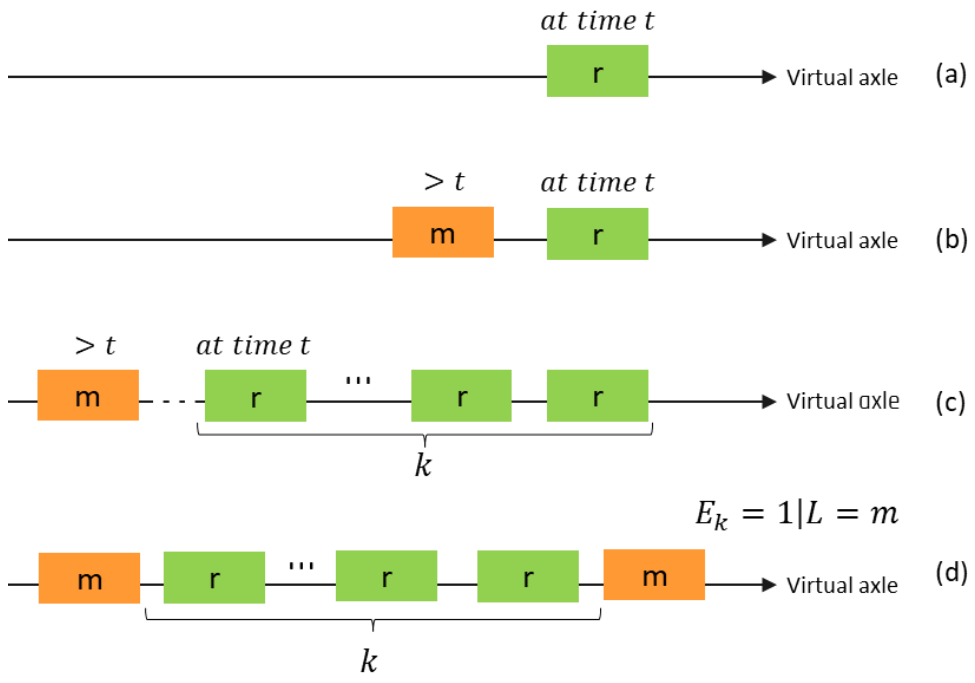

FIG. 5-4. Schematic diagram of the proof steps

Proof. As shown in **FIG 5-4 (a)**, let's first assume there's a vehicle just passed the point before time t, and followed by this vehicle, an on-ramp vehicle also passed this point at time t. Based on the definition of exponential distribution and assumption made above, the probability of this on-ramp CAV_r passing through the merging point at time t can be calculated as:

$$\Pr(CAV_r = t) = \lambda_r e^{-\lambda_r t}. \tag{70}$$

On this basis, follow by the on-ramp vehicle, if a mainline vehicle also passed this point after time t, shown as **FIG 5-4 (b)**, the corresponding probability of the whole process can be expressed as:

$$\Pr(CAV_{\mathrm{m}} > t | CAV_r = t) \tag{71}$$

$$= \int_0^{\infty} P(CAV_m > t) f(CAV_r = t) dt$$

$$= \int_0^{\infty} \left(1 - \left(1 - e^{-\lambda_m t}\right)\right)\left(\lambda_r e^{-\lambda_r t}\right) dt \; = -\frac{\lambda_r}{\lambda_m + \lambda_r} e^{-(\lambda_m + \lambda_r)t} |_0^{\infty}$$

$$= \frac{\lambda_r}{\lambda_m + \lambda_r}.$$

Next, as shown in **FIG. 5-4 (c)**, what happened if k numbers of consecutive on-ramp vehicles passing through this point at time t? Based on the definition, since each vehicle passing a point at a certain amount of time follows an exponential distribution, the summation of k numbers of consecutive vehicles follows an Erlang distribution. Thus, the probability of (c) can be formulated as:

$$\Pr(CAV_m > t | Erlang(k, \lambda_r) = t) \tag{72}$$

$$= \int_0^{\infty} \left(1 - \left(1 - e^{-\lambda_m t}\right)\right) * \frac{\lambda_r^k t^{k-1}}{(k-2)!} e^{-\lambda_r t} dt$$

$$= \int_0^{\infty} \frac{\lambda_r^k t^{k-1}}{(k-1)!} e^{-\lambda_r t} e^{-\lambda_m t} dt \; = \frac{{\lambda_r}^k}{(k-1)!} \int_0^{\infty} t^{k-1} e^{-(\lambda_m + \lambda_r)t} dt$$

$$= \frac{{\lambda_r}^k}{(k-1)!} * \frac{(k-1)!}{(\lambda_m + \lambda_r)^k} = \left(\frac{\lambda_r}{\lambda_m + \lambda_r}\right)^k.$$

Then, based on the property of memoryless-ness of the exponential distribution, the probability of a topology subset that first and last vehicle coming from the mainline and k vehicles in between coming from the on-ramp, as shown in **FIG. 5-4 (d)**, can be expressed as:

$$\Pr(E_k = 1 | L = m) \tag{73}$$

$$= \Pr\left(CAV_{m,first}\right) * \Pr(CAV_m > t | Erlang(k, \lambda_r)$$

$$= t) * \Pr\left(CAV_{m,last}\right) = \left(\frac{\lambda_r}{\lambda_m + \lambda_r}\right)^k * \left(\frac{\lambda_m}{\lambda_m + \lambda_r}\right)^2.$$

Therefore, in other words, the general events that the first vehicle is coming from the mainline can be indicated as Eq. (73).

Similarly, we can have the expression of probability for the other general event type that first and last vehicle comes from on-ramp:

Lemma 1. The conditional probability of E_k happened when the first and last CAVs in the topology subset is coming from the on-ramp follows,

$$\Pr(E_k = 1|L = r) = \left(\frac{\lambda_m}{\lambda_m + \lambda_r}\right)^k * \left(\frac{\lambda_r}{\lambda_m + \lambda_r}\right)^2. \tag{74}$$

After deriving the probability of both types, we can easily have lemma 2 as follow:

Lemma 2. Based on the two types of probability equation, the probability of a general event E_k happened is determined by the sum of the $E_k = 1|L = m$ and $E_k = 1|L = r$. Thus, according to Eqs. (69) and (74), we can get:

$$\begin{aligned}\Pr(E_k = 1) &= [\Pr(E_k = 1|L = m) + \Pr(E_k = 1|L = r)] \\ &= \left(\frac{\lambda_r}{\lambda_m + \lambda_r}\right)^k * \left(\frac{\lambda_m}{\lambda_m + \lambda_r}\right)^2 + \left(\frac{\lambda_m}{\lambda_m + \lambda_r}\right)^k * \left(\frac{\lambda_r}{\lambda_m + \lambda_r}\right)^2 \\ &= \frac{{\lambda_m}^k {\lambda_r}^2 + {\lambda_r}^k {\lambda_m}^2}{(\lambda_m + \lambda_r)^{k+2}}.\end{aligned} \tag{75}$$

Note that, the special event will be included in the following expected τ calculation.

Now, the PMF of arrival pattern has been determined, by combining both PMF of communication capability and arrival pattern, we can further determine the expected τ in proposition 5.

Proposition 5. The expected τ in the on-ramp merging scenario can be expressed as:

$$\Pr\left(\tau_{min,k+1}\right) = \begin{cases} 1 - \sum_{k=1}^{N_{max}-1} \frac{{\lambda_m}^k {\lambda_r}^2 + {\lambda_r}^k {\lambda_m}^2}{(\lambda_m + \lambda_r)^{k+2}} * \Pr(N_{i,cap} \geq k+1), & k = 0 \\ \frac{{\lambda_m}^k {\lambda_r}^2 + {\lambda_r}^k {\lambda_m}^2}{(\lambda_m + \lambda_r)^{k+2}} * \Pr\left(N_{i,cap} \geq k+1\right), 1 \leq \forall k \leq N_{max} - 1 \end{cases} . \tag{76}$$

where the upper formula represents the probability of special event with 0 in-between vehicles. Note that the $\Pr(N_{i,cap} \geq k+1)$ illustrate the probability of allowed communicated predecessors that obey the MLT rules.

Proposition 6. Further, based on the definition of expected value, the expected capacity (long-term average) for on-ramp merging scenario can be formulated as:

$$\begin{aligned} \mathrm{E}[\mathrm{C}_{or}] = \sum_{k=1}^{N_{max}-1} C_k \left(\frac{{\lambda_m}^k {\lambda_r}^2 + {\lambda_r}^k {\lambda_m}^2}{(\lambda_m + \lambda_r)^{k+2}} * \Pr\left(N_{i,cap} \geq k+1\right) \right) \\ + C_1 \left(1 - \sum_{k=1}^{N_{max}-1} \frac{{\lambda_m}^k {\lambda_r}^2 + {\lambda_r}^k {\lambda_m}^2}{(\lambda_m + \lambda_r)^{k+2}} * \Pr(N_{i,cap} \geq k+1) \right). \end{aligned} \tag{77}$$

where $\mathrm{E}[\mathrm{C}_{or}]$ represents the expected capacity for on-ramp scenario, C_k denotes the corresponding capacity of topology subset that with k number of in-between vehicles, C_1 denotes the capacity of topology subset that with 0 in-between vehicles.

Proposition 7. Similarly, the corresponding variance of the expected capacity follows:

$$\begin{aligned} Var(C_{or}) &= \mathrm{E}[\mathrm{C}_{or}^2] - \mathrm{E}[\mathrm{C}_{or}]^2 \\ &= \left[\sum_{k=1}^{N_{max}-1} C_k^2 \left(\frac{{\lambda_m}^k {\lambda_r}^2 + {\lambda_r}^k {\lambda_m}^2}{(\lambda_m + \lambda_r)^{k+2}} * \Pr\left(N_{i,cap} \geq k+1\right) \right) + C_1^2 \left(1 \right. \right. \\ &\quad \left. \left. - \sum_{k=1}^{N_{max}-1} \frac{{\lambda_m}^k {\lambda_r}^2 + {\lambda_r}^k {\lambda_m}^2}{(\lambda_m + \lambda_r)^{k+2}} * \Pr\left(N_{i,cap} \geq k+1\right) \right) \right] - \mathrm{E}[\mathrm{C}_{or}]^2. \end{aligned} \tag{78}$$

Some special property can be determined from the above formulae as follow:

Proposition 8. When $k \geq 2$, $\varepsilon_m = \frac{1}{2}$ is the global stationary point (maxima) of the expected capacity equation in Eq. (77).

Proof. To further simplify the above equations, we defined the expected arrival rate ratio $\varepsilon_m = \frac{\lambda_m}{\lambda_m+\lambda_r}$, and $\frac{\lambda_r}{\lambda_m+\lambda_r} = 1 - \varepsilon_m$. Then, the proposition 6 can be get as below:

$$\begin{aligned} \mathrm{E}[\mathrm{C}_{or}] = \sum_{k=0}^{N_{max}-1} C_k \left({\varepsilon_m}^{k+2} + (1-\varepsilon_m)^{k+2}\right) * \Pr\left(N_{i,cap} \geq k+1\right) \\ + C_1 \Big(1 \\ - \sum_{k=0}^{N_{max}-1} \left({\varepsilon_m}^{k+2} + (1-\varepsilon_m)^{k+2}\right) * \Pr\left(N_{i,cap} \geq k+1\right)\Big). \end{aligned} \tag{79}$$

Then, to find the local stationary points of expected capacity function, we apply Fermat's theorem (Fletcher, 1989) by different Eq. (79) as follow:

$$\begin{aligned} \frac{\partial \mathrm{E}[\mathrm{C}_{or}]}{\partial \varepsilon_m} = \sum_{k=0}^{N_{max}-1} C_k \left({\varepsilon_m}^{k+2} + (1-\varepsilon_m)^{k+2}\right) * \Pr\left(N_{i,cap} \geq k+1\right) \\ + C_1 \left(1 - \sum_{k=0}^{N_{max}-1} \left({\varepsilon_m}^{k+2} + (1-\varepsilon_m)^{k+2}\right) * \Pr\left(N_{i,cap} \geq k+1\right)\right) \\ = \sum_{k=0}^{N_{max}-1} \Pr\left(N_{i,cap} \geq k+1\right) C_k \, (k+2) {\varepsilon_m}^{k+1} (1-\varepsilon_m)^{k+2} \\ - \sum_{k=0}^{N_{max}-1} \Pr\left(N_{i,cap} \geq k+1\right) C_k {\varepsilon_m}^{k+2} (k+2) \, (1-\varepsilon_m)^{k+1} \\ - \sum_{k=0}^{N_{max}-1} \Pr\left(N_{i,cap} \geq k+1\right) C_1 \, (k+2) {\varepsilon_m}^{k+1} (1-\varepsilon_m)^{k+2} \\ + \sum_{k=0}^{N_{max}-1} \Pr\left(N_{i,cap} \geq k+1\right) C_1 {\varepsilon_m}^{k+2} (k+2) (1-\varepsilon_m)^{k+1} \\ = \sum_{k=0}^{N_{max}-1} \Pr\left(N_{i,cap} \geq k+1\right) (k+2) \, (\varepsilon_m - \varepsilon_m^2)^{k+1} (C_k - C_1)(1 \\ - 2\varepsilon_m). \end{aligned} \tag{80}$$

Let $\frac{\partial\,\mathbb{E}(\mathrm{C})}{\partial\varepsilon_m}=0$, we can easily calculate the only root is when ε_m equal to $\frac{1}{2}$, thus, the point is global stationary. Then, to find whether this root (stationary point) is maxima or minima, we take the second derivative of Eq. (80) as below:

$$\begin{aligned}\frac{\partial^2\mathrm{E}[\mathrm{C}_{or}]}{\partial{\varepsilon_m}^2}&=\frac{\partial}{\partial\varepsilon_m}\sum_{k=0}^{N_{max}-1}\Pr\left(N_{i,cap}\geq k+1\right)(k+2)\,(\varepsilon_m-\varepsilon_m^2)^{k+1}(C_k-C_1)(1\\&\quad-2\varepsilon_m)\\&=\sum_{k=0}^{N_{max}-1}\frac{\partial}{\partial\varepsilon_m}\Pr\left(N_{i,cap}\geq k+1\right)(k+2)(\varepsilon_m-\varepsilon_m^2)^{k+1}(C_k\\&\quad-C_1)(1-2\varepsilon_m)\\&=\sum_{k=0}^{N_{max}-1}\Pr\left(N_{i,cap}\geq k+1\right)(k+2)\,(C_k-C_1)((\varepsilon_m-\varepsilon_m^2)^k(k\\&\quad+1)(1-2\varepsilon_m)^2-2(\varepsilon_m-\varepsilon_m^2)^{k+1}).\end{aligned}\tag{81}$$

Since we assume $\Pr\left(N_{i,cap}\geq k+1\right)$ is a known constant value, and by substituting ε_m with $\frac{1}{2}$, and let $k\geq 2, C_k-C_1>0$, we have:

$$\sum_{k=0}^{N_{max}-1}(k+2)\,(C_k-C_1)\left(-2(0.25)^{k+1}\right)<0\tag{82}$$

Since the Eq. (8282) illustrates that the second derivative of expected capacity equation is negative when ε_m is $\frac{1}{2}$, we can conclude that local stationary point is maxima which means when the expected arriving rate ratio between mainline and on-ramp is 50/50, the expected capacity reaches maximum.

To summarize, we have designed a stochastic capacity model for on-ramp merging scenario based on the high-dimensional parameters including control gains, traffic arrival pattern, and communication capability. Specifically, both traffic arrival pattern and communication capability are the stochastic feature in this model.

6. NUMERICAL EXPERIMENTS FOR STOCHASTIC CAPACITY ANALYSIS

This chapter presents the numerical experiments for the impact of multi-scale parameters on the stochastic capacity. Specifically, based on the formulae we designed in **Chapter 5**, we mainly divided the sensitivity analysis into three categories as: 1) control gain scale; 2) communication capability scale; 3) traffic arrival pattern scale. Each scale is discussed separately through the following session. Note that all the simulations are all conducted on MATLAB.

6.1 Simulation Setting

Since the on-ramp merging stochastic capacity model we designed is a function with respect of traffic condition (initial velocity), control gains (ω_e,ω_v), communication loss (P, α, β, O), and traffic arrival pattern (λ_m, λ_r). Thus, to theoretically understand the impact of these high-dimensional parameter on the road capacity. We have carefully chosen the default values and reasonable interval range for each parameter in order to best illustrate the influence. The default value settings are listed in **Table 6-1**. Specifically, we set the τ_{safe} as 0.3 sec and initial velocity as 27 m/s (60 mi/hr). For stochastic features, the normal distribution for noise is set to 0 means with 0.2 standard deviation; and the normal distribution for operation error is set to 0 means with 2 meters standard deviation. The exponential distribution rate parameter for mainline and on-ramp are set as 1.5 and 0.5, which means when there are 3 vehicles passing from the mainline, one vehicle will pass from the on-ramp. Note that both normal and exponential distribution are numerically generated in the software.

Table 6-1. Default value setting for the stochastic capacity sensitivity analysis

Parameter	Notation	Value
Equilibrium Spacing Coefficient	$\omega_{e,max}$	1.2
Equilibrium Speed Coefficient	$\omega_{v,min}$	0.5
Maximum Communication Capability	N_{max}	5
Initial Velocity (m/s)	V_{int}	27
Transmission Power (mW)	P	1000

Signal Power Decay	α	2
Noise Normal Distribution	(μ_O, σ_O)	(0,0.2)
Operation Error Normal Distribution	(μ_Q, σ_Q)	(0,2)
Threshold	β	0.45
Exponential Distribution Rate Parameter for Mainline	λ_m	1.5
Exponential Distribution Rate Parameter for On-ramp	λ_r	0.5
Safe Desire Time Gap (sec)	τ_{safe}	0.3

6.2 Control Gain Scale

To deeply understand the impact of the proposed merging controller on traffic throughput, we set the control gains parameter ω_e from 1.05 to 1.4, and ω_v from 0.35 to 0.7. All the other parameters shown in **Table 6-1** remain the same. The corresponding expected capacity and variance result have shown in **FIG 6-1**. It is seemed that the maximum capacity is around 8000 (vehphpl) as shown in the upper right corner. Based on the color gradient, the capacity increase when ω_e is larger and ω_v is smaller. This trend meet our expectation since based on the relationship we determined from the string stability criterion, the desired time gap τ is small when ω_e is large and ω_v is small. Similarly, the standard deviation shows the same trends as the expected capacity.

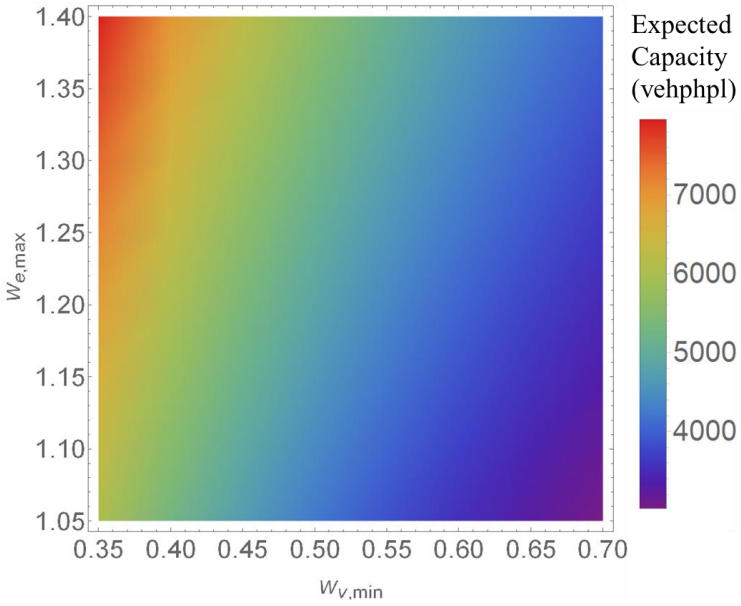

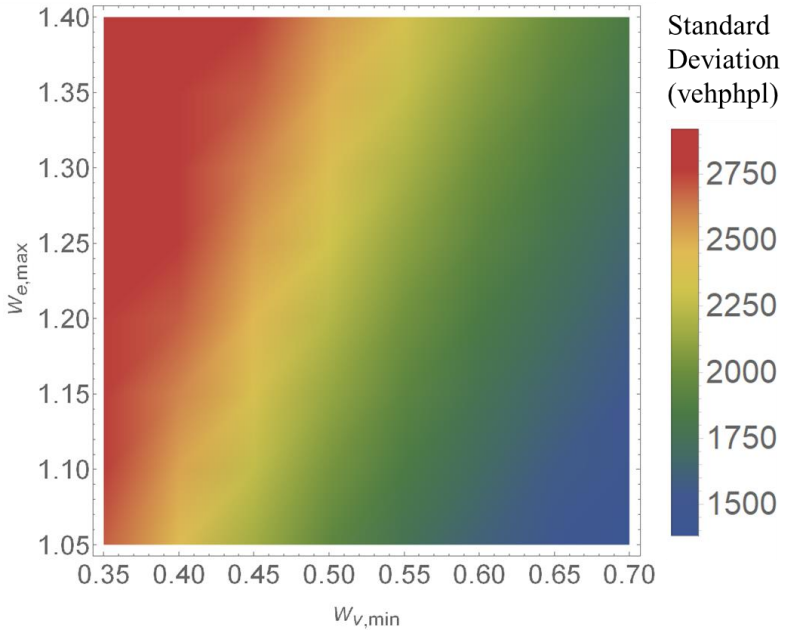

FIG. 6-1. Expected capacity and variance result for control gain scale

6.3 Communication Capability Scale

As we mentioned in **Chapter 5**, capacity is strongly related to the stochasticity of communication capability. Thus, in order to systematically analyze the impact of parameters in SINR calculation on capacity, in this experiment, we have selected three major parameters including transmission power P, signal decay rate α and threshold β as the sensitivity analysis targets.

6.3.1 Transmission Power Versus Signal Power Decay

Start with the transmission power and signal power decay, we have set the transmission power from 500 to 3000 megawatts and decay from 0.5 to 3. The expected capacity and variance results have been shown in **FIG. 6-2**. The maximum sustainable flow rate is around 5000 on the left side of the figure. By the color gradient, the capacity increase when power is strong, and decay is small. But take a closer look, the capacity is much sensitive with decay than with the power. The main reason of this trends may be explained as when every vehicle in the control range has strong transmission power, the power may be offset by each other. Further, the standard deviation shows the same trends as the expected capacity.

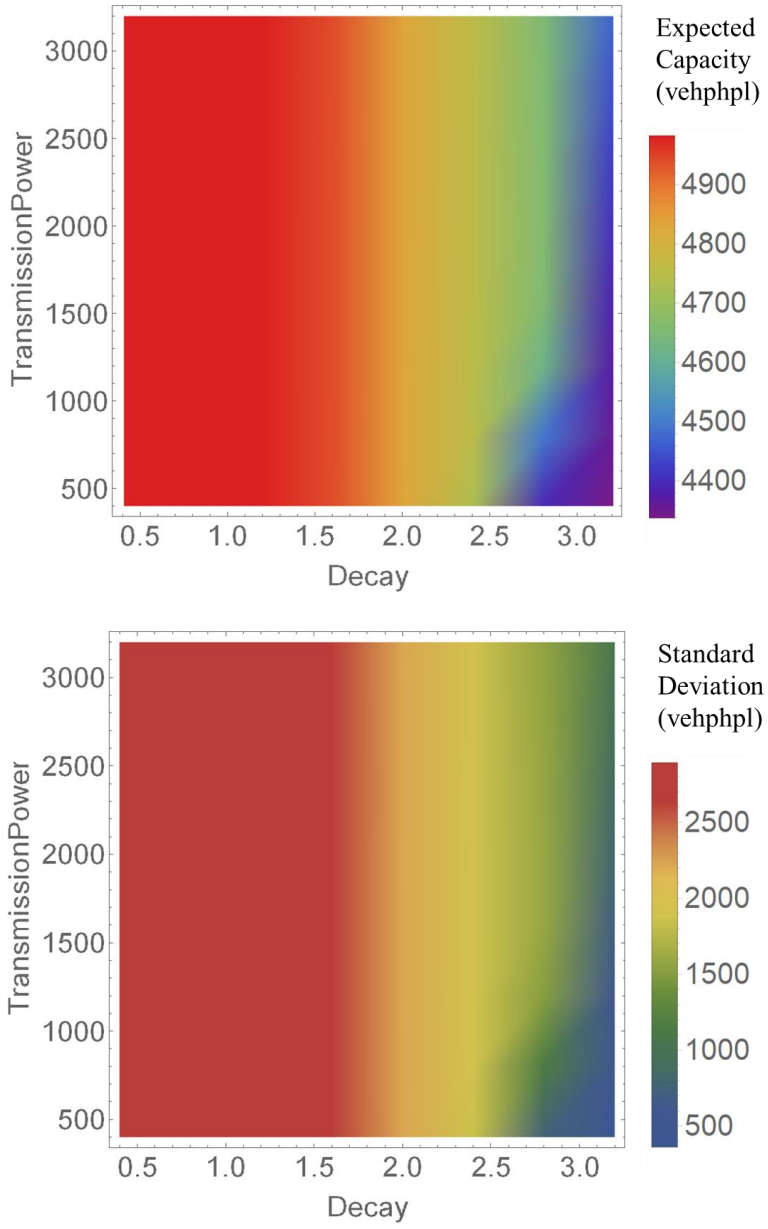

FIG. 6-2. Expected capacity and variance result for communication capability Scale: Transmission power VS Decay

6.3.2 Threshold Versus Signal Power Decay

The next sensitivity analysis for communication capability is threshold versus signal power decay. Thus, we have set the threshold interval from 0.02 to 0.12 and decay from 0.5 to 3. The corresponding expected capacity and variance results have been shown in **FIG. 6-3**. The maximum sustainable flow

rate is around 5000 in the right lower corner. By the color gradient, the capacity increase when threshold is small, and decay is small, which make sense. Since the threshold is directly response to whether the connection between vehicles is allowed or not. Smaller threshold allows more vehicles to communicate. Thus, based on the proposed control strategy, more communicated vehicle within one communication topology decreases the corresponding τ which increase the capacity. Overall, for communication factors, capacity increase when transmission power is strong, signal decay and threshold is small.

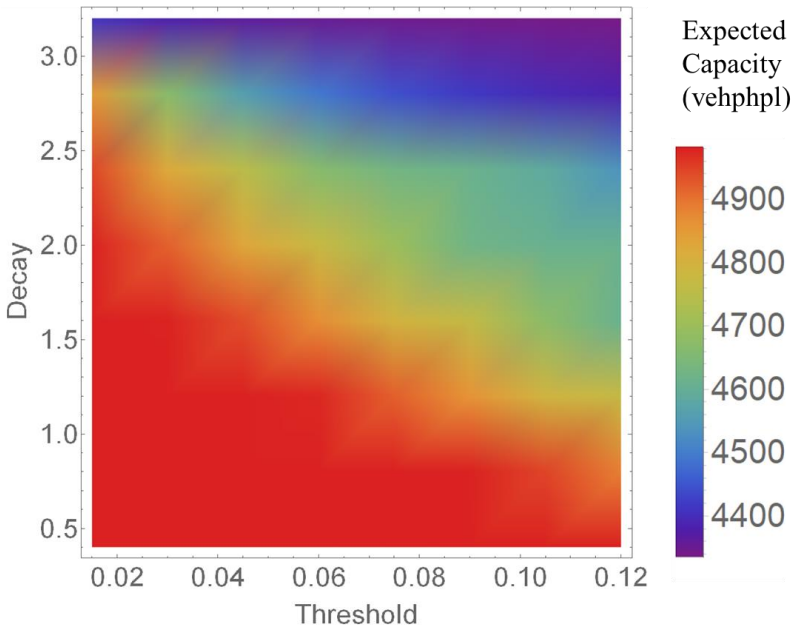

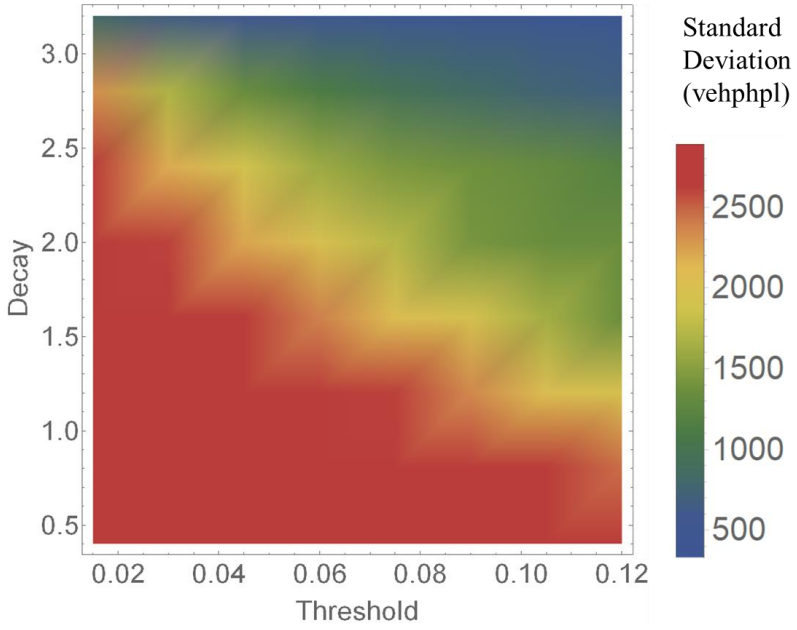

FIG. 6-3. Expected capacity and variance result for communication capability Scale: Threshold VS Decay

6.4 Traffic Arrival Pattern Scale

To analyze the impact of different traffic arrival rate on both mainline and on-ramp, and to verify the proposition 6 and 8, we set the expected arriving rate ratio ε_m as [0.1:0.9] to generate the expected capacity and standard deviation. The corresponding result with respect to ε_m is shown in **FIG. 6-4**. It is observed that with the ε_m increasing, both capacity and standard deviation curve show the symmetric concave down slope with global maxima point at $\varepsilon_m = \frac{1}{2}$ which verify the proposition 8. Thus, in reality, the optimal traffic throughput under the proposed merging controller is when the mainline traffic flow and on-ramp traffic flow ratio is 50/50.

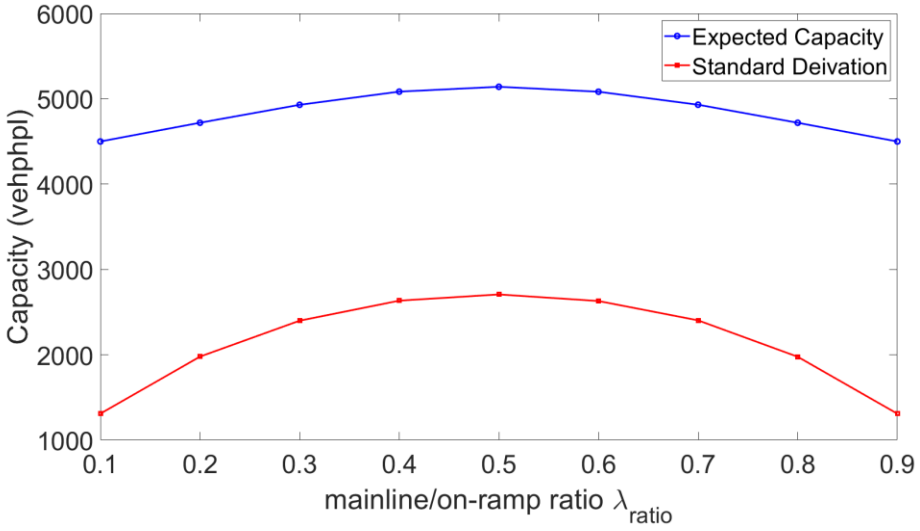

FIG. 6-4. Expected capacity and variance result for traffic arrival pattern scale

7. CONCLUSION

7.1 Summary of Chapters

Chapter 1 introduced the background of traffic congestion and emerging technologies and pointed out the importance to system-wisely utilize the CAV techniques to improve traffic efficiency and safety in complex scenarios. This chapter further illustrated the problem statement and listed all objectives and assumptions of this research.

Chapter 2 summarized existing studies on CAV control under on-ramp merging scenario and CAV capacity analysis. For the CAV merging microscopic control, most studies mainly proposed their unique strategy to control the vehicle actively create gaps to ensure merging safety. However, some of the early works ignored to reduce the voids, and most of them ignored the cause of traffic oscillation which increase safety risk. Especially, they lacked a mathematical framework and methods to theoretically analyze the system stability for the merging process. For the CAV capacity analysis, research mainly used deterministic method to estimate the CAV capacity characteristics. However, the effect of CAV stochasticity factor had rarely been addressed. And for complex scenarios such as merging had not been analyzed.

Chapter 3 utilized a virtual rotation concept to reformulate the problem as a ‘virtual’ CF problem by assuming the ramp is straight. Based on that, a communication topology and corresponding cooperative control model on the shared virtual lane had been proposed. For rigor, a string stability criterion had been mathematically proved for the ‘virtual’ CF problem. Then, we relaxed the assumption of the straightness of the ramp and developed a local lateral controller by extending the ramp scenario to a two-dimensional path coordinate.

Chapter 4 provided numerical simulation experiments to analyze the practicality and effectiveness of the proposed rotation-based CAV merging control algorithm. The result proves that the proposed controllers can actively reduce the void and meanwhile guarantee the damping of traffic oscillations in

the merging control area.

Chapter 5 designed a unified framework incorporating multiple factors to understand the parametric impacts on the stochastic capacity. By utilizing the microscopic control strategy, we first exploited a CF capacity estimation model by introducing communication capability stochastic factor, and further formulated an on-ramp merging capacity estimation model by adding traffic arrival pattern stochastic factors. Specifically, the expected capacity and corresponding variance equations for CAV at on-ramp merging have been designed based on the three high-dimensional factors: 1) control gains, 2) communication capability, 3) traffic arrival pattern.

Chapter 6 discussed the impact of multi-scale high-dimensional parameters on the stochastic on-ramp merging capacity model based on numerical analysis. The result shows that the capacity is strongly related to CAV control gains, communication capability and traffic arrival pattern.

7.2 Conclusions

This study proposes a systematic framework for CAV control at on-ramp merging scenario from microscopic vehicle controller to macroscopic capacity analysis. The framework mainly divided into two parts. For the first part, a novel cooperative merging control strategy of CAVs based on a virtual rotation approach has been designed. Specifically, the virtual rotation strategy has been introduced which project CAVs on mainline and CAVs on on-ramp to a shared straight axis, which greatly simplified the problem to a virtual car following problem while maintaining all characteristic of concern. By using the merge point as a reference, a virtual car following sequences of vehicles is generated by integrating the virtual rotation and FIFO rules, which serves as an upper-level controller. A unidirectional multi-leader communication topology is specifically designed to fully utilize the downstream CAVs information and achieve the strict string stability for the on-ramp lane and mainstream lane. With the proposed topology, we design a multiple-predecessor feedback and feedforward longitudinal controller and derived sufficient conditions for the string stability criterion

with two case studies: 1) Equally weighted predecessors information case, 2) Non-equally weighted predecessors information case. Further, to expand the application scenarios, we design a local-based lateral controller based on an extended linear-quadratic regulator in a path coordinate system for the curvy ramp lane case. Two sets of numerical simulation experiments are conducted to verify the efficiency and stability for the system. For longitudinal controller experiments, 12-CAV trajectories portfolio including position, speed, acceleration, and energy have been conducted to validate the model. The results reveal that the proposed controller can actively reduce the voids and meanwhile guarantee the distribution attenuation of the whole system. Similarly, for the lateral control experiment, the result elucidates reasonably well to guarantee the smoothness of the turning movements with the small-angle approximation. For the second part, a stochastic capacity analysis has been designed to understand multiple factor impact. By utilizing first part works, we formulated CF capacity modelling and on-ramp merging capacity modelling based on three high-level factors including control gains, communication capabilities, and traffic arrival pattern. Then numerical simulations are conducted to illustrate the impact on different stochastic factors.

To the best of our acknowledgment, it is the first attempt using the virtual rotation concept to turn a two-dimensional merging problem into a one-dimensional CF control problem for multi-vehicle controller with mathematical proofs of string stability criterion. And one of the earliest efforts on two-dimensional extension for merging and CAV on-ramp capacity analysis in a stochastic manner. The result of this study not only proposed a well-defined control strategy that ensure safety and smooth the traffic dynamics, but also perform rigorous mathematical modeling of the problem to theoretically illustrate properties.

7.3 Future Works

Some future works are desired on the results of this study. For example, for the microscopic analysis, future work could consider systematic car sequencing optimization to further improve the performance in this paper. We could incorporate uncertainties in vehicle dynamics and potential communication

delays into robust control design. In addition, for the macroscopic analysis, more complex scenarios such as intersection, roundabout, multi-lanes can be considered. Further, mixed traffic could be considered as an extension in the future.

REFERENCE

Ahn, S, & Cassidy, M. J. (2007). Freeway traffic oscillations and vehicle lane-change maneuvers. *Proceedings of the 17th International Symposium on Traffic and Transportation Theory*.

Ahn, Soyoung, Laval, J., & Cassidy, M. J. (2010). Effects of merging and diverging on freeway traffic oscillations. *Transportation Research Record*, *2188*, 1–8. https://doi.org/10.3141/2188-01

Akpakwu, G. A., Silva, B. J., Hancke, G. P., & Abu-Mahfouz, A. M. (2017). A Survey on 5G Networks for the Internet of Things: Communication Technologies and Challenges. In *IEEE Access*. https://doi.org/10.1109/ACCESS.2017.2779844

Anderson, B. D. O., & Moore, J. B. (2007). *Optimal control: linear quadratic methods*. Courier Corporation.

Anstett, N., & Kühne, R. (1999). *Focker Planck Desciption of traffic pattern formation*.

Arfken, G. B., Weber, H. J., & Harris, F. E. (2013). Mathematical Methods for Physicists. In *Mathematical Methods for Physicists*. https://doi.org/10.1016/C2009-0-30629-7

Bian, Y., Zheng, Y., Ren, W., Li, S. E., Wang, J., & Li, K. (2019). Reducing time headway for platooning of connected vehicles via V2V communication. *Transportation Research Part C: Emerging Technologies*, *102*(March), 87–105. https://doi.org/10.1016/j.trc.2019.03.002

Brilon, W., Geistefeldt, J., & Zurlinden, H. (2007). Implementing the concept of reliability for highway capacity analysis. *Transportation Research Record*, *2027*, 1–8. https://doi.org/10.3141/2027-01

Cao, W., Mukai, M., Kawabe, T., Nishira, H., & Fujiki, N. (2015). Cooperative vehicle path generation during merging using model predictive control with real-time optimization. *Control Engineering Practice*. https://doi.org/10.1016/j.conengprac.2014.10.005

Carlson, R. C., Papamichail, I., Papageorgiou, M., & Messmer, A. (2010a). Optimal mainstream traffic flow control of large-scale motorway networks. *Transportation Research Part C: Emerging Technologies*, *18*(2), 193–212. https://doi.org/10.1016/j.trc.2009.05.014

Carlson, R. C., Papamichail, I., Papageorgiou, M., & Messmer, A. (2010b). Optimal motorway traffic flow control involving variable speed limits and ramp metering. *Transportation Science*, *44*(2), 238–253. https://doi.org/10.1287/trsc.1090.0314

Cassidy, M. J., & Rudjanakanoknad, J. (2005). Increasing the capacity of an isolated merge by metering its on-ramp. *Transportation Research Part B: Methodological*, *39*(10), 896–913. https://doi.org/10.1016/j.trb.2004.12.001

Chen, D., & Ahn, S. (2018). Capacity-drop at extended bottlenecks: Merge, diverge, and weave. *Transportation Research Part B: Methodological*, *108*, 1–20. https://doi.org/10.1016/j.trb.2017.12.006

Chen, D., Ahn, S., Chitturi, M., & Noyce, D. A. (2017). Towards vehicle automation: Roadway capacity formulation for traffic mixed with regular and automated vehicles. *Transportation Research Part B: Methodological*, *100*, 196–221.

Chen, N., van Arem, B., Alkim, T., & Wang, M. (2020). A Hierarchical Model-Based Optimization Control Approach for Cooperative Merging by Connected Automated Vehicles. *IEEE Transactions on Intelligent Transportation Systems*, 1–14. https://doi.org/10.1109/tits.2020.3007647

Chen, T., Wang, M., Gong, S., Zhou, Y., & Ran, B. (2021). Connected and automated vehicle distributed control for on-ramp merging scenario: A virtual rotation approach. *Transportation Research Part C: Emerging Technologies*, *133*, 103451. https://doi.org/https://doi.org/10.1016/j.trc.2021.103451

Darbha, S., Konduri, S., & Pagilla, P. R. (2017). Effects of V2V communication on time headway for autonomous vehicles. *Proceedings of the American Control Conference*. https://doi.org/10.23919/ACC.2017.7963246

Darbha, Swaroop, Konduri, S., & Pagilla, P. R. (2019). Benefits of V2V communication for autonomous and connected vehicles. *IEEE Transactions on Intelligent Transportation Systems*.

https://doi.org/10.1109/TITS.2018.2859765

Davis, L. C. (2007). Effect of adaptive cruise control systems on mixed traffic flow near an on-ramp. *Physica A: Statistical Mechanics and Its Applications*. https://doi.org/10.1016/j.physa.2006.12.017

de Waard, D., Dijksterhuis, C., & Brookhuis, K. A. (2009). Merging into heavy motorway traffic by young and elderly drivers. *Accident Analysis and Prevention*. https://doi.org/10.1016/j.aap.2009.02.011

Ding, F., Ran, B., Cheng, Y., Li, S., Zhang, Z., Zhou, Y., Tan, H., Dong, S., Chen, T., & Li, X. (2019). *Systems and methods for driving intelligence allocation between vehicles and highways*. Google Patents.

Du, L., & Dao, H. (2014). Information dissemination delay in vehicle-to-vehicle communication networks in a traffic stream. *IEEE Transactions on Intelligent Transportation Systems*, *16*(1), 66–80.

Duret, A., Wang, M., & Ladino, A. (2019). A hierarchical approach for splitting truck platoons near network discontinuities. *Transportation Research Procedia*, *38*, 627–646.

Elefteriadou, L., Roess, R. P., & McShane, W. R. (1995). Probabilistic nature of breakdown at freeway merge junctions. *Transportation Research Record*, *1484*, 80–89.

Fletcher, C. R. (1989). Fermat's theorem. *Historia Mathematica*, *16*(2), 149–153.

Ghiasi, A., Hussain, O., Qian, Z. (Sean), & Li, X. (2017). A mixed traffic capacity analysis and lane management model for connected automated vehicles: A Markov chain method. *Transportation Research Part B: Methodological*, *106*, 266–292. https://doi.org/https://doi.org/10.1016/j.trb.2017.09.022

Gong, S., & Du, L. (2018). Cooperative platoon control for a mixed traffic flow including human drive vehicles and connected and autonomous vehicles. *Transportation Research Part B: Methodological*. https://doi.org/10.1016/j.trb.2018.07.005

Gong, S., Shen, J., & Du, L. (2016). Constrained optimization and distributed computation based car following control of a connected and autonomous vehicle platoon. *Transportation Research Part B: Methodological*. https://doi.org/10.1016/j.trb.2016.09.016

Greenshields, B. D., Thompson, J. T., Dickinson, H. C., & Swinton, R. S. (1934). The photographic method of studying traffic behavior. *Highway Research Board Proceedings*, *13*.

Han, Y., & Ahn, S. (2018). Stochastic modeling of breakdown at freeway merge bottleneck and traffic control method using connected automated vehicle. *Transportation Research Part B: Methodological*, *107*, 146–166. https://doi.org/10.1016/j.trb.2017.11.007

Kachroo, P., & Li, Z. (1997). Vehicle merging control design for an automated highway system. *IEEE Conference on Intelligent Transportation Systems, Proceedings, ITSC*, 224–229. https://doi.org/10.1109/itsc.1997.660479

KiM. (2015). *Mobility Report 2015*. 182. http://web.minienm.nl/mob2015/documents/Mobiliteitsbeeld_2015.pdf

Lancaster, P., & Rodman, L. (1995). *Algebraic riccati equations*. Clarendon press.

Laval, J. A., & Daganzo, C. F. (2006). Lane-changing in traffic streams. *Transportation Research Part B: Methodological*. https://doi.org/10.1016/j.trb.2005.04.003

Li, X., Peng, F., & Ouyang, Y. (2010). Measurement and estimation of traffic oscillation properties. *Transportation Research Part B: Methodological*. https://doi.org/10.1016/j.trb.2009.05.003

Lorenz, M. R., & Elefteriadou, L. (2001). Defining freeway capacity as function of breakdown probability. *Transportation Research Record*, *1776*, 43–51. https://doi.org/10.3141/1776-06

Lu, X. Y., Tan, H. S., Shladover, S. E., & Hedrick, J. K. (2004). Automated Vehicle Merging Maneuver Implementation for AHS. *Vehicle System Dynamics*. https://doi.org/10.1076/vesd.41.2.85.26497

McCartt, A. T., Northrup, V. S., & Retting, R. A. (2004). Types and characteristics of ramp-related motor vehicle crashes on urban interstate roadways in Northern Virginia. *Journal of Safety Research*. https://doi.org/10.1016/j.jsr.2003.09.019

Metropolis, N., & Ulam, S. (1949). The monte carlo method. *Journal of the American Statistical Association*, *44*(247), 335–341.

Milanes, V., Shladover, S. E., Spring, J., Nowakowski, C., Kawazoe, H., & Nakamura, M. (2014). Cooperative adaptive cruise control in real traffic situations. *IEEE Transactions on Intelligent Transportation Systems*, *15*(1), 296–305. https://doi.org/10.1109/TITS.2013.2278494

Mobility, E. (2018). *Wisconsin Transportation by the Numbers SAFE , SMOOTH AND EFFICIENT MOBILITY*. *September*.

Morbidi, F., Colaneri, P., & Stanger, T. (2013). Decentralized optimal control of a car platoon with guaranteed string stability. *2013 European Control Conference (ECC)*, 3494–3499.

Necsulescu, D., Pruner, E., Sasiadek, J., & Kim, B. (2010). Control of nonholonomic autonomous vehicles and their formations. *2010 15th International Conference on Methods and Models in Automation and Robotics, MMAR 2010*, *1*, 37–42. https://doi.org/10.1109/MMAR.2010.5587268

Ntousakis, I. A., Porfyri, K., Nikolos, I. K., & Papageorgiou, M. (2014). Assessing the impact of a cooperative merging system on highway traffic using a microscopic flow simulator. *ASME International Mechanical Engineering Congress and Exposition, Proceedings (IMECE)*. https://doi.org/10.1115/IMECE2014-39850

Ozguven, E. E., & Ozbay, K. (2008). Nonparametric Bayesian estimation of freeway capacity distribution from censored observations. *Transportation Research Record*, *2061*(1), 20–29.

Papageorgiou, M., Hadj-Salem, H., & Middelham, F. (1997). ALINEA local ramp metering: Summary of field results. *Transportation Research Record*. https://doi.org/10.3141/1603-12

Papageorgiou, M., Papamichail, I., Spiliopoulou, A. D., & Lentzakis, A. F. (2008). Real-time merging traffic control with applications to toll plaza and work zone management. *Transportation Research Part C: Emerging Technologies*, *16*(5), 535–553. https://doi.org/10.1016/j.trc.2007.11.002

Persaud, B., Yagar, S., & Brownlee, R. (1998). Exploration of the breakdown phenomenon in freeway traffic. *Transportation Research Record*, *1634*(1), 64–69.

Puwal, S., & Roth, B. J. (2007). Forward Euler stability of the bidomain model of cardiac tissue. *IEEE Transactions on Biomedical Engineering*, *54*(5), 951–953. https://doi.org/10.1109/TBME.2006.889204

Rajamani, R., Tan, H. S., Law, B. K., & Zhang, W. bin. (2000). Demonstration of integrated longitudinal and lateral control for the operation of automated vehicles in platoons. *IEEE Transactions on Control Systems Technology*, *8*(4), 695–708. https://doi.org/10.1109/87.852914

Ran, B., Cheng, Y., Li, S., Ding, F., Jin, J., Chen, X., & Zhang, Z. (2019). *Connected automated vehicle highway systems and methods*. Google Patents.

Ran, B., Leight, S., & Chang, B. (1999). A microscopic simulation model for merging control on a dedicated-lane automated highway system. *Transportation Research Part C: Emerging Technologies*, *7*(6), 369–388. https://doi.org/10.1016/S0968-090X(99)00028-5

Rios-Torres, J., Malikopoulos, A., & Pisu, P. (2015). Online Optimal Control of Connected Vehicles for Efficient Traffic Flow at Merging Roads. *IEEE Conference on Intelligent Transportation Systems, Proceedings, ITSC*. https://doi.org/10.1109/ITSC.2015.392

SAE. (2016). Automated Driving - Levels of Driving Automation Are Defined in New Sae International Standard J3016. In *SAE international*.

Schmidt, G. K., & Posch, B. (1983). A two-layer control scheme for merging of automated vehicles. *The 22nd IEEE Conference on Decision and Control*, 495–500.

Sendra, J. R., & Winkler, F. (1991). Symbolic parametrization of curves. *Journal of Symbolic Computation*, *12*(6), 607–631.

Singh, A. K., & Pal, B. C. (2017). An extended linear quadratic regulator for LTI systems with exogenous inputs. *Automatica*. https://doi.org/10.1016/j.automatica.2016.10.014

Shi, H., Zhou, Y., Wu, K., Wang, X., Lin, Y., & Ran, B. (2021). Connected automated vehicle cooperative control with a deep reinforcement learning approach in a mixed traffic environment. *Transportation Research Part C: Emerging Technologies*, *133*, 103421.

Sridhar, B., Grabbe, S. R., & Mukherjee, A. (2008). Modeling and Optimization in Traffic Flow Management. *Proceedings of the IEEE*, *96*(12), 2060–2080. https://doi.org/10.1109/JPROC.2008.2006141

Steele, J. M. (2004). *The Cauchy-Schwarz master class: an introduction to the art of mathematical inequalities*. Cambridge University Press.

Talebpour, A., & Mahmassani, H. S. (2016). Influence of connected and autonomous vehicles on traffic flow stability and throughput. *Transportation Research Part C: Emerging Technologies*, *71*, 143–163. https://doi.org/10.1016/j.trc.2016.07.007

van Arem, B., van Driel, C. J. G., & Visser, R. (2006). The impact of cooperative adaptive cruise control on traffic-flow characteristics. *IEEE Transactions on Intelligent Transportation Systems*, *7*(4), 429–436. https://doi.org/10.1109/TITS.2006.884615

Wang, C., Gong, S., Zhou, A., Li, T., & Peeta, S. (2020). Cooperative adaptive cruise control for connected autonomous vehicles by factoring communication-related constraints. *Transportation Research Part C: Emerging Technologies*. https://doi.org/10.1016/j.trc.2019.04.010

Wang, M. (2018). Infrastructure assisted adaptive driving to stabilise heterogeneous vehicle strings. *Transportation Research Part C: Emerging Technologies*. https://doi.org/10.1016/j.trc.2018.04.010

Wang, M., Daamen, W., Hoogendoorn, S. P., & van Arem, B. (2016). Cooperative Car-Following Control: Distributed Algorithm and Impact on Moving Jam Features. *IEEE Transactions on Intelligent Transportation Systems*, *17*(5), 1459–1471. https://doi.org/10.1109/TITS.2015.2505674

Wang, M., Treiber, M., Daamen, W., Hoogendoorn, S. P., & van Arem, B. (2013). Modelling Supported Driving as an Optimal Control Cycle: Framework and Model Characteristics. *Procedia - Social and Behavioral Sciences*, *80*, 491–511. https://doi.org/10.1016/j.sbspro.2013.05.027

Wang, Z., Kulik, L., & Ramamohanarao, K. (2007). Proactive traffic merging strategies for sensor-enabled cars. *VANET'07: Proceedings of the Fourth ACM International Workshop on Vehicular Ad Hoc Networks*. https://doi.org/10.1145/1287748.1287755

Zhou, M., Qu, X., & Li, X. (2017). A recurrent neural network based microscopic car following model to predict traffic oscillation. *Transportation Research Part C: Emerging Technologies*, *84*, 245–264. https://doi.org/https://doi.org/10.1016/j.trc.2017.08.027

Zheng, Z., Ahn, S., Chen, D., & Laval, J. (2011). Freeway traffic oscillations: Microscopic analysis of formations and propagations using Wavelet Transform. *Transportation Research Part B: Methodological*. https://doi.org/10.1016/j.trb.2011.05.012

Zhou, Y., & Ahn, S. (2019). Robust local and string stability for a decentralized car following control strategy for connected automated vehicles. *Transportation Research Part B: Methodological*. https://doi.org/10.1016/j.trb.2019.05.003

Zhou, Y., Ahn, S., Chitturi, M., & Noyce, D. A. (2017). Rolling horizon stochastic optimal control strategy for ACC and CACC under uncertainty. *Transportation Research Part C: Emerging Technologies*. https://doi.org/10.1016/j.trc.2017.07.011

Zhou, Y., Ahn, S., Wang, M., & Hoogendoorn, S. (2020). Stabilizing mixed vehicular platoons with connected automated vehicles: An H-infinity approach. *Transportation Research Part B:*

Methodological. https://doi.org/10.1016/j.trb.2019.06.005